

# A Lagrangian subgridscale model for particle transport improvement and application in the Adriatic Sea using the Navy Coastal Ocean Model

Angelique C. Haza<sup>a</sup>, Leonid I. Piterbarg<sup>b</sup>, Paul Martin<sup>c</sup>,  
Tamay M. Özgökmen<sup>a,\*</sup>, Annalisa Griffa<sup>a,d</sup>

<sup>a</sup> *RSMASIMPO, University of Miami, Miami, FL, USA*

<sup>b</sup> *CAMS, University of Southern California, Los Angeles, CA, USA*

<sup>c</sup> *Naval Research Laboratory, Stennis Space Center, MS, USA*

<sup>d</sup> *Consiglio Nazionale delle Ricerche, ISMAR, LaSpezia, Italy*

Received 3 May 2006; received in revised form 27 October 2006; accepted 30 October 2006

Available online 22 December 2006

---

## Abstract

An accurate estimation of Lagrangian transport in the ocean is important for a number of practical problems such as dispersion of pollutants, biological species, and sediments. Forecasting of the Lagrangian pathways necessarily relies on the accuracy of ocean and coastal models. However, these models include a number of errors that propagate directly from the Eulerian velocity field to the Lagrangian transport.

In this study, so-called Lagrangian sub-grid-scale, or LSGS, model is developed to reduce errors projected to Lagrangian transport from errors arising from missing physics, uncertainties in forcing and unresolved scales in OGCMs. The LSGS method acts on the diagnostics of particle transport computed from coastal or ocean models, and it allows to minimize the discrepancy between the statistical behavior of the modeled (synthetic) and real (observed) trajectories. The method is shown to work well using both a so-called Markov velocity field model, representing an idealized turbulent flow field, and in the context of the Navy Coastal Ocean Model (NCOM) configured in the Adriatic Sea for realistic, high-resolution, complex ocean flows.

The simplicity and computational efficiency of this technique, combined with applicability to ocean models at a wide range of resolutions, appears promising in light of the challenge of capturing exactly the oceanic turbulent fields, which is critical for Lagrangian dispersion.

© 2006 Elsevier Ltd. All rights reserved.

---

## 1. Introduction

Ocean general circulation models (OGCMs) are providing increasingly more realistic Eulerian velocity fields (e.g., Smith et al., 2000; Garraffo et al., 2001; McClean et al., 2002). Subsequently, there has been

---

\* Corresponding author.

E-mail address: [tozgokmen@rsmas.miami.edu](mailto:tozgokmen@rsmas.miami.edu) (T.M. Özgökmen).

a development of operational programs that rely on the assimilation of various observational data in ocean circulation models to forecast the ocean state (e.g., Pinardi et al., 2003). Realistic ocean and coastal model results are then used for a number of practical applications, such as ship navigation and the estimation of the dispersion of pollutants, biological species, and sediments. At the basis of such applications is the transport of a passive tracer field and/or particles. It is this particular transport problem that poses significant computational challenges and is the focus of the present investigation.

Motivated by the increase in the number of drifters and floats released in the oceans in the last few decades (e.g., Davis, 1991; Owens, 1991; Fratantoni, 2001; Richardson, 2001; Zhang et al., 2001; Lavender et al., 2002; Bauer et al., 2003; Zhou et al., 2002; Reverdin et al., 2003), the theoretical treatment of the Lagrangian transport problem has received much attention. Two general theoretical approaches have been developed to understand and model the Lagrangian transport. The first is a statistical approach, which is motivated by the work of Thomson (1986) and was pioneered for oceanic applications by Griffa (1996). In this approach, the two-dimensional flow field is decomposed into a mean and eddy velocity, in which the eddy Lagrangian velocity is modeled as a Markov process satisfying the so-called Langevin equation or random-flight model. This Lagrangian stochastic model is represented by a first-order, linear, ordinary differential equation, the parameters of which, namely the velocity variance and correlation time, can be estimated using drifter data sets. It has been shown by Falco et al. (2000) that such models can be useful for approximating realistic particle motion. Other versions of such stochastic models have been developed, namely higher-order models (Berloff and McWilliams, 2002), multi-particle models (Piterburg, 2001a,b), and models that take into account the motion due to trapping in mesoscale vortices (Veneziani et al., 2005a,b). Each of these advances requires additional parameters (for instance, the spatial decorrelation scale and spin parameter in the latter two cases) that need to be estimated from oceanic drifter data. Another variation is to assimilate drifter data in such Lagrangian models to help predict particle motion (Özgökmen et al., 2000, 2001; Castellari et al., 2001). To summarize, the main concept in these studies relies on a stochastic process to generate simulated trajectories using a model, the parameters of which are estimated statistically from existing data sets. One of the fundamental problems associated with this approach is the decomposition into a mean and eddy component, which, similar to the Reynolds decomposition, implies that the eddy component represents *all* turbulent scales. Given the high Reynolds number of oceanic flows exhibiting coherent structures at a wide range of scales due to many interacting processes, the underlying assumption of Brownian flow in such models is idealistic.

A completely different, namely purely deterministic, approach has been developed based on dynamical system theory. These techniques focus on identifying coherent structures geometrically, in particular, so-called hyperbolic trajectories in the Lagrangian frame, which are characterized by the intersection of a stable manifold (along which fluid particles are attracted toward the hyperbolic point) and an unstable manifold (along which fluid particles are repelled away from the hyperbolic point) from a velocity field displaying complex time variability (Wiggins, 2005). One of the issues regarding the calculation of these manifolds is that infinite data are required both forward and backward in time, which is clearly impractical for oceanic applications. Haller and Poje (1998) focused on the transient stagnation points and finite-time analogs of stable and unstable manifolds, and extended the lobe analysis to the treatment of finite-time data. This method was then used to analyze fluid particle pathways in an eddy resolving, barotropic model (Poje and Haller, 1999). Finite-time geometric techniques have been successful in locating the boundaries of mesoscale coherent features in the Lagrangian frame (e.g., Coulliette and Wiggins, 2000; Miller et al., 2002). It has also been shown that seeding observations in rapidly stretching regions of the flow field in the vicinity of hyperbolic trajectories leads to improvement of the reconstruction of Eulerian fields from Lagrangian data (Poje et al., 2002; Toner and Poje, 2004) and in the performance of a Lagrangian data assimilation scheme (Molcard et al., 2006). However, only persistent, coherent structures can be captured by such geometric techniques and flow regimes with no or highly-transient coherent structures cannot be handled effectively. The most critical aspect of this approach is the total reliance of the Lagrangian transport map on the accuracy of the simulated Eulerian velocity fields.

The modeled Eulerian field produced by the OCGMs cannot be entirely accurate because of three fundamental reasons. First, the model *forcing* via wind stress, heat flux, precipitation, evaporation, and boundary conditions introduces errors due to space and time sparseness of the observational data sets and inaccuracies in the larger-scale coupled simulation. Second, ocean and coastal models typically contain *missing physics*. For

instance, flow interaction with capes and headlands, which are ubiquitous coastal features, can introduce stratified mixing and high vertical velocities (e.g., Farmer et al., 2002; Pawlak et al., 2003), which cannot be handled within the context of the hydrostatic approximation generally employed in such models. Surface mixed layers include a range of nonhydrostatic stratified mixing processes and air–sea interaction problems (Kantha and Clayson, 2000) that pose great challenges for circulation models. Third, given that circulation models are discretized in such a way that not all scales of motion are resolved (typical mesh spacings at the present time are 100 km in climate models, 10 km in general circulation models, and 1 km in coastal models), there is the issue of the effect of *unresolved or filtered scales*. For instance, most OCGMs use Laplacian or biharmonic subgridscale operators for momentum and active tracers, which are ultimately based on the studies by Taylor (1921) and Kolmogoroff (1941) of laboratory-scale flow behavior. There are no oceanic observations to support the validity of such a generic down-gradient flux assumption or to accurately estimate the value of the eddy viscosity and diffusivity as a function of the mesh spacing. In contrast, the development of high-frequency Doppler radar for coastal observations revealed submesoscale (2–3 km in diameter) eddies (Shay et al., 2000), the parameterization of which differs significantly from that based on eddy-viscosity models (Caglar et al., 2006). Finally, the fractal nature of the Earth's morphology (Weissel et al., 1994) implies unresolved topography at even the smallest scales.

Thus, it is clear that OCGMs can only provide an approximate Eulerian velocity field representing the coastal and ocean circulation. Given that drifters feel forces acting on the scale of their physical size, namely  $O(1\text{ m})$  (and similar considerations for other passive particles), their transport with the flow field generated by numerical models will be subject to a range of errors that can significantly affect their paths and dispersion (as implied by the results presented in Griffa et al., 2004). Since such circulation models are computationally expensive and will continue to contain similar errors in the foreseeable future, how can their Lagrangian transport characteristics be improved in a cost-effective and realistic manner?

Here, we put forth and explore a simple method as a first step toward addressing this problem. The main underlying idea is to determine and minimize the discrepancy between the statistical behavior of the modeled and real trajectories. A simple model, referred to as a Lagrangian sub-grid-scale (LSGS) model hereafter, is then developed to reduce this discrepancy. The method is based on the use of stochastic models, but differently from previous works (e.g. Griffa, 1996; Berloff and McWilliams, 2002) in which the focus was on characterizing the action of the *entire* eddy field, here the final goal is to isolate and parameterize only that part of the eddy field which is not correctly captured and reproduced by the numerical circulation model. The approach is inherently statistical, and differs, for instance, from the data assimilation approach, in which Lagrangian observations are used to improve prediction of a specific realization of velocity or trajectories (e.g., Özgökmen et al., 2000; Molcard et al., 2003; Taillandier et al., 2006). Here, the focus is on particle statistics associated with a given Eulerian velocity, which is improved using information from observational statistics. The LSGS model is capable of producing ensemble particle trajectories from given initial conditions, providing information on tracer dispersion or, equivalently, on the maps of probability of finding a particle at a given point. Alternatively, this method can be viewed as the Lagrangian counterpart of the so-called large-eddy-simulation method (Sagaut, 2005), in which the main concept is to incorporate the effect of the unresolved turbulence on the resolved turbulent motion by adding SGS stresses to the Eulerian momentum equations. These SGS stresses are tuned to be consistent with physical insight (e.g., the Kolmogoroff turbulent energy spectrum) or with results from fully-resolved simulations. In our case, the LSGS model represents the terms added to the Lagrangian advection model such that particle advection is modified to be consistent with the behavior of observed trajectories in the statistical sense.

The method is tested in three stages. First, a Lagrangian stochastic model in the context of the Langevin equation, a random-flight model, is employed to model the Lagrangian eddy field to confirm that the LSGS model acts to restore the statistical properties of the observed/reference particle motion. The random-flight model generates particle trajectories based on input statistical parameters, such as the turbulent velocity fluctuation and correlation time scale, without the need of an underlying Eulerian velocity field. Thus, it is a first ideal testbed. However, the correction by the LSGS model in the context of the random-flight model does not take into account the effect of the *local* model fields. Thus, a so-called Markov velocity-field model, representing the behavior of an idealized, two-dimensional, turbulent velocity field, is employed to test a space-dependent version of the method. Finally, the LSGS model is applied to rectify the particle transport based on

hourly output from a realistic, high-resolution (1-km) ocean model, the Navy Coastal Ocean Model (NCOM), configured in the Adriatic Sea. The LSGS technique offers two significant advantages. The first is the fundamental issue that it can be applied to numerical models at all resolutions, since the principle of the LSGS model is to correct the errors in the Lagrangian transport due to the effect of unresolved scales of motion, missing physics, and forcing errors. The second is that the LSGS model can be used on the transport diagnostics from post-processed (low-pass filtered) coastal or ocean model outputs. In other words, existing Eulerian output can be employed in conjunction with this technique in order to obtain a more realistic particle transport, without the need to rerun the circulation model. The main requirement (and possible drawback) is that an observational drifter data set of adequate coverage (space/time density) is needed to improve the modeled Lagrangian transport in the area of interest.

The paper is organized as follows: The theory leading to the LSGS is provided in Section 2. The proof of the LSGS model formula and details of the Markov velocity field model are given in Appendix A. NCOM is described in Section 3. The results from both the Markov velocity field model and NCOM are presented in Section 4. The conclusions and directions for future work are discussed in Section 5.

## 2. Theory of the Lagrangian subgridscale model

Lagrangian motion in a random or even complex deterministic velocity field can be described as a stochastic process. Thus, its full description is given by a joint probability distribution of velocities and positions of any number of particles for any set of time moments. It is not realistic to estimate or derive theoretically this distribution in any region of the world ocean for now or in the future. To this end, only the statistical characteristics of one-particle motion have been extensively studied (e.g., Veneziani et al., 2004; and references cited therein) and some efforts have been carried out toward two-particle motion (e.g., LaCasce and Bower, 2000; LaCasce and Ohlmann, 2003). Thus, in this paper we focus on the statistics of single-particle motion characterized by a joint pdf  $p(t, \mathbf{v}, \mathbf{r})$  of the velocity  $\mathbf{v}$  and position  $\mathbf{r}$  at moment  $t$ . Recall that the one-particle motion pdf completely determines the mean concentration  $\bar{c}(\mathbf{r})$  of a passive scalar, while the two-particle statistics allow finding the spatial covariance tensor of the concentration field. In particular, for an incompressible, inviscid flow and a delta-function source,  $\bar{c}(\mathbf{r})$  is obtained by integration of the pdf over  $\mathbf{v}$ .

In turn, an OGCM produces an ensemble of Lagrangian trajectories characterized by the model pdf  $p_m(t, \mathbf{v}, \mathbf{r})$ . For numerous reasons indicated in Section 1,  $p_m(t, \mathbf{v}, \mathbf{r})$  turns out to be quite different from  $p(t, \mathbf{v}, \mathbf{r})$ . Therefore a typical OGCM is not able to reproduce dispersion of a passive scalar with high accuracy. A natural question is whether a model trajectory ensemble can be corrected in a way to approximately retrieve the real pdf  $p(t, \mathbf{v}, \mathbf{r})$ . The most obvious correction would be the addition of another stochastic process to the model velocity to compensate for the effect of missing physics and scales. Thus, the simplest mathematical formulation of a LSGS model is as follows.

**Problem 1.** Let  $\mathbf{v}(t), \mathbf{v}_m(t)$  be the real and model sample Lagrangian velocities, respectively, of a single particle in the time interval  $[0, T]$ . Find a random vector process, the SGS or missing velocity component,  $\boldsymbol{\eta}(t)$ , such that the corrected position and velocity defined by

$$d\mathbf{r}_c(t)/dt = \mathbf{v}_c(t), \quad \mathbf{v}_c(t) = \mathbf{v}_m(t) + \boldsymbol{\eta}(t) \quad (1)$$

have the same pdf  $p(t, \mathbf{v}, \mathbf{r})$  as a real particle provided with the same initial condition, for each time moment  $t \in [0, T]$ .

Thus, by inserting the missing component, one can improve the prediction of tracer spreading.

In a significant part of the world ocean, individual Lagrangian trajectories on horizontal or isopycnal surfaces can be described, at least to first approximation, by the first-order Markov or random-flight model (see again Veneziani et al., 2004; Falco et al., 2000)

$$d\mathbf{r} = (\mathbf{V}(t, \mathbf{r}) + \mathbf{v}') dt, \quad d\mathbf{v}' = -A\mathbf{v}' dt + A d\mathbf{w}, \quad (2)$$

where  $\mathbf{V}(t, \mathbf{r}(t))$  is the deterministic drift,  $\mathbf{v}'$  is the fluctuation velocity with zero mean driven by standard 2D Brownian motion  $\mathbf{w}$ . The dissipation and dispersion matrices are given by

$$A = \begin{pmatrix} 1/\tau_u & \Omega \\ -\Omega & 1/\tau_v \end{pmatrix}, \quad A = \begin{pmatrix} \sigma_u \sqrt{2/\tau_u} & 0 \\ 0 & \sigma_v \sqrt{2/\tau_v} \end{pmatrix}, \quad (3)$$

where  $\sigma_u$ ,  $\sigma_v$  are the rms of the zonal and meridional velocity fluctuations, respectively,  $\tau_u$ ,  $\tau_v$  are the corresponding Lagrangian correlation times, and  $\Omega$  is the spin.

The model was first developed for Lagrangian motion in the atmosphere by Thomson (1986), and the concept of spin was introduced by Borgas et al. (1997) and Reynolds (2002, 2003). A remarkable fact is that in the framework of (2), the aforementioned pdf  $p(t, \mathbf{v}, \mathbf{r})$  is completely determined by the initial conditions, the drift  $\mathbf{V}(t, \mathbf{r})$ , the turbulent velocity variance  $\sigma$ , the Lagrangian correlation time  $\tau$ , and the spin  $\Omega$ . More exactly, this pdf can be found as a solution of the corresponding Fokker–Planck equation given the listed parameters.

The basic assumption behind our approach is the following:

**Assumption 1.** Both the real and model single-particle trajectories are well approximated by model (2,3) with the same drift  $\mathbf{V}$  and different fluctuation parameters  $\sigma$ ,  $\tau$ ,  $\Omega$ .

Under this assumption, which in particular implies that the model is capable of exactly capturing the drift, Problem 1 can be reformulated as follows:

**Problem 2.** Let  $\mathbf{v}'_r(t)$  and  $\mathbf{v}'_m(t)$  be the real and model Lagrangian fluctuation velocities of a single particle, respectively, and described by the same Langevin equation in (2) with different parameters. Find a random vector process (missing component)  $\eta(t)$  such that the corrected velocity fluctuation

$$\mathbf{v}'_c(t) = \mathbf{v}'_m(t) + \eta(t) \quad (4)$$

is covered by the Langevin equation with real parameters.

In other words, we want the corrected velocity and position to satisfy (2) with real parameters, but of course with another (say independent) Brownian forcing since the goal is to reproduce just the real statistics rather than an individual trajectory itself. This problem formulation requires knowledge of the real fluctuation parameters. In addition, it is natural to require the missing component to be completely determined only by the model trajectory (plus, of course, the statistics of the real trajectories).

A solution of the formulated problem is given by the following statement. Introduce

$$C_r(x) = xI + A_r, \quad C_m(x) = xI + A_m, \quad Q(x) = A_r C_r(x) A_r^{-1}, \quad P(x) = A_r C_m(x) A_m^{-1} - Q(x),$$

where matrices  $A_r$ ,  $A_r$  and  $A_m$ ,  $A_m$  are defined by (3) for real and model parameters, respectively,  $I$  is the  $2 \times 2$  unit matrix, and  $x$  is a dummy variable.

**Proposition 1.** Let the 2D process  $\eta(t)$  be a solution of the following stochastic differential equation

$$Q\left(\frac{d}{dt}\right)\eta = P\left(\frac{d}{dt}\right)\mathbf{v}'_m. \quad (5)$$

Then, the corrected velocity defined by (4) satisfies the equation for the real velocity in (2), thereby yielding a solution of Problem 2.

The proof is given in Appendix A.1. If both spins are zero,  $\Omega_r = \Omega_m = 0$ , then (5) breaks down into two separate identical equations for each component. The equation for the zonal direction becomes:

$$\frac{d\eta}{dt} = a \frac{du'_m}{dt} + bu'_m + c\eta, \quad (6)$$

where

$$a = \frac{\sigma_r \sqrt{\tau_m}}{\sigma_m \sqrt{\tau_r}} - 1, \quad b = \frac{\sigma_r}{\sigma_m \sqrt{\tau_r \tau_m}} - \frac{1}{\tau_r}, \quad c = -\frac{1}{\tau_r}. \quad (7)$$

Now subscripts  $r$ ,  $m$  denote real and model, respectively. In particular, the variance (energy) of the missing component  $\eta$  in the stationary case is given by

$$\overline{\eta^2} = \frac{(\sigma_r \sqrt{\tau_m} - \sigma_m \sqrt{\tau_r})^2 + (\sigma_r \sqrt{\tau_r} - \sigma_m \sqrt{\tau_m})^2}{\tau_r + \tau_m}, \quad (8)$$

which is zero if the model and real parameters coincide.

The correlation coefficient  $r_{mc}$  between the modeled and corrected velocity also can be found from (6), (7) (see Appendix A.2). It is interesting that it depends only on the ratio  $\gamma = \tau_m/\tau_r$  of the model and real Lagrangian time scales and has a simple analytical expression, namely

$$r_{mc} = \frac{2\sqrt{\gamma}}{1 + \gamma}.$$

In particular, for  $1/4 \leq \gamma \leq 4$  we have  $r_{mc} \geq 0.8$ . That high correlation is well illustrated by the experiments following below.

To ensure stationarity of the LSGS component  $\eta(t)$ , the initial condition  $\eta(0)$  should be taken as a normal random value with zero mean and with variance given by (8). For long enough realizations,  $\eta(t)$  becomes stationary for  $t \gg \tau_r$  for arbitrary initial conditions.

To illustrate how the suggested procedure of adding the LSGS component performs, we first experiment with a simplified version of the model (2), in which the mean drift is zero and the variances of the zonal and meridional components are equal, as well as the correlation times, for both the real and model flows. The scheme of the simulations is as follows. Given a set of the real  $\sigma_r, \tau_r, \Omega_r$  and model  $\sigma_m, \tau_m, \Omega_m$  parameters, the real and model velocities and corresponding trajectories are generated via (2). Then, by solving (6) or (5) (if the spin is not zero), the LSGS component is computed and inserted by (1). Finally, the corrected and real trajectories (velocities) are compared visually and statistically.

In Fig. 1, an example of the model real and corrected velocities ( $u$ -component) are shown for an integration time period of  $T = 100$  days and parameter values  $\sigma_r = 20$  cm/s,  $\tau_r = 6$  days,  $\Omega_r = 0$ ,  $\sigma_m = 10$  cm/s,  $\tau_m = 1.5$  days, and  $\Omega_m = 0$ . Since the spin is equal to zero, we used Eq. (6). It can be seen that the corrected velocity has energy values and fluctuation scales closer to the real ones with respect to the model velocity, while it is well correlated with the latter. The parameters estimated from the corrected velocity,

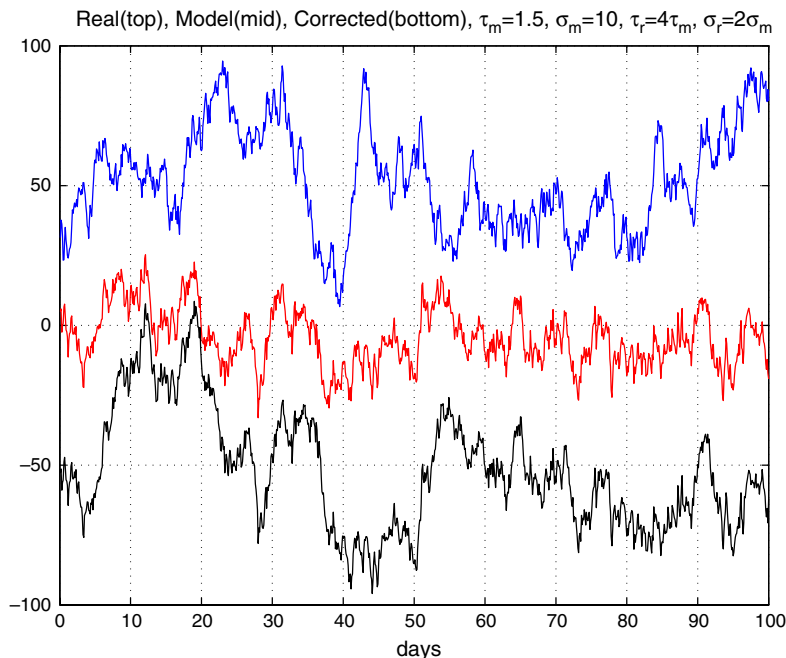


Fig. 1. Time series of model (red), real (blue), and corrected (black) velocities. The time series of the real (corrected) velocities is shifted by  $50 \text{ cm s}^{-1}$  upwards (downwards) to better demonstrate their differences. In particular, note that the LSGS model acts to enhance the amplitude of the model velocity fluctuations to be more consistent with the real case. The means of all three time series are zero.

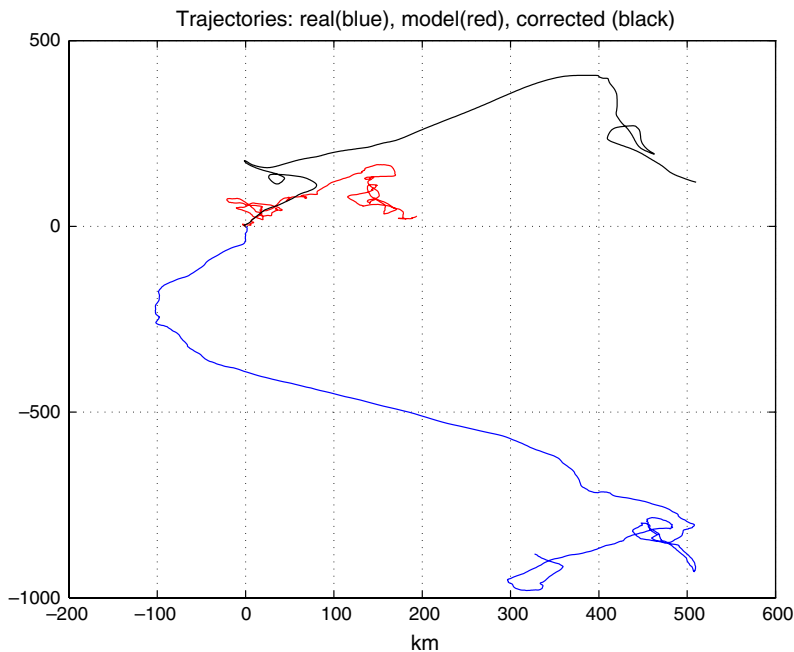


Fig. 2. Model (red), real (blue), and corrected (black) trajectories.

$\sigma_c = 20.8$  cm/s and  $\tau_c = 5.16$  days, are close to the real values. The corresponding model trajectory is much shorter than the real one due to the deficit of energy while the corrected one is approximately of the same length as the real trajectory (Fig. 2).

Another experiment with smaller velocities and non-zero real spin with  $\sigma_r = 1$  cm/s,  $\tau_r = 3.5$  days,  $\Omega_r = 2\pi/20$ ,  $\sigma_m = 0.25$  cm/s,  $\tau_m = 10$  days, and  $\Omega_m = 0$  shows that the LSGS algorithm is able to reproduce loops observed in the real trajectory even though there are no loops in the model trajectory (Fig. 3).

Notice that so far, there is no explicit spatial structure of the motion involved in our approach. The LSGS procedure given by (6) or (5) is, in fact, a posterior procedure, since a Lagrangian trajectory is first computed over the whole time interval  $[0, T]$  and then Eq. (6) or (5) is solved in the same interval. Thus, no adjustment to the factual position of the particle is suggested, which can be misleading if the particle motion in a velocity field is considered. As an alternative, we present the so called *space-dependent* LSGS model as follows.

First, we introduce the model Eulerian velocity field (say zonal component) and assume a constant drift

$$u_m(t, \mathbf{r}) = U + u'_m(t, \mathbf{r}).$$

The assumption is due to difficulties arising from the separation of Lagrangian motion into deterministic drift and fluctuations for a non-constant mean flow, say  $\mathbf{U}(t, \mathbf{r})$ . More exactly, the problem is that in this case the drift  $\mathbf{V}(t, \mathbf{r})$  introduced in (2) is not equal to  $\mathbf{U}(t, \mathbf{r})$  at all, and moreover, cannot be expressed explicitly in terms of  $\mathbf{U}$  and the statistics of  $\mathbf{u}'$ . Then rewrite the Eqs. (6) and (1) for the corrected velocity and zonal component of position in a slightly different form:

$$\frac{d\eta(t)}{dt} = a \frac{du'_m(t, \mathbf{r}_m(t))}{dt} + bu'_m(t, \mathbf{r}_m(t)) + c\eta(t), \quad \frac{dx_c(t)}{dt} = U + u'_m(t, \mathbf{r}_m(t)) + \eta(t). \quad (9)$$

The suggested space-coordinate dependent procedure is obtained by replacing  $\mathbf{r}_m(t)$  in (9) with  $\mathbf{r}_c(t)$ , i.e.:

$$\frac{d\eta(t)}{dt} = a \frac{du'_m(t, \mathbf{r}_c(t))}{dt} + bu'_m(t, \mathbf{r}_c(t)) + c\eta(t), \quad \frac{dx_c(t)}{dt} = U + u'_m(t, \mathbf{r}_c(t)) + \eta(t). \quad (10)$$

This formula, together with an obvious replica for the meridional component, is a basis for implementing the LSGS model in a space-dependent model. In the following, we will test it using both a synthetic random velocity field and NCOM. While proof for the random-flight model is given in Appendix A.1, we cannot present a

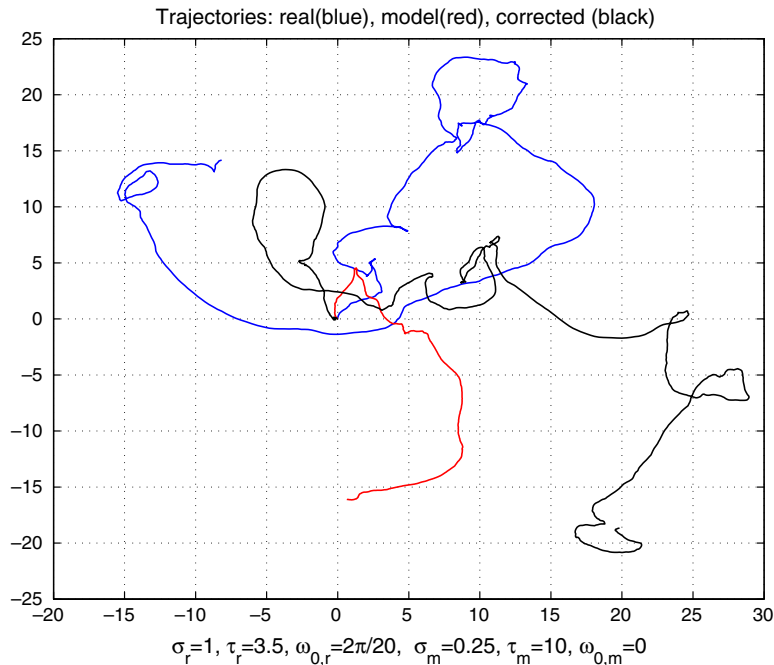


Fig. 3. Model (red), real (blue), and corrected (black) trajectories, in the case where missing spin is added by the LSGS model.

proof for the case of a random Markov velocity field model that the statistics of the corrected trajectories (via Eq. (10) in this case) are identical to those of the real trajectories. It is probably a hard mathematical problem since an analysis of the space-dependent procedure requires taking into consideration the spatial structure of the velocity field. For this reason, the procedure has been thoroughly tested with numerical simulations. As will be seen later, the conjecture will turn out to be well supported by the simulations.

### 3. Navy Coastal Ocean Model

The ocean model used for this study is the Navy Coastal Ocean Model (NCOM) as described in [Martin \(2000\)](#), with some improvements as described in [Morey et al. \(2003\)](#) and [Barron et al. \(2006\)](#). This is a hydrostatic model, which is similar in its physics and numerics to the Princeton Ocean Model (POM) ([Blumberg and Mellor, 1987](#)), but uses an implicit treatment of the free surface and a hybrid vertical grid with sigma coordinates in the upper layers and (optionally) level coordinates below a user-specified depth.

The model equations include a source term that can be used for river inflows. A third-order upwind method ([Holland et al., 1998](#)) was used for advection. Vertical mixing was computed using the Mellor–Yamada Level 2 scheme ([Mellor and Yamada, 1974](#)). The equation of state used was that of [Mellor \(1991\)](#).

The ocean model domain consists of the entire Adriatic Sea, a sub-basin of the Mediterranean Sea, and it includes the Strait of Otranto and a small part of the northern Ionian Sea. The horizontal grid resolution is 1019.5 m. The vertical grid consists of 32 total layers, with 22 sigma layers used from the surface down to a depth of 291 m and level coordinates used below 291 m. Hence, the grid is like a regular sigma coordinate grid in water shallower than 291 m and similar to a level grid in deeper water. The vertical grid is uniformly stretched from the surface downward with a maximum thickness of the upper layer of 2 m and a maximum depth of 1262 m.

Initial conditions and daily boundary conditions (BC) were taken from a hindcast of a global model ([Barron et al., 2004](#)). The numerical treatment of the BC includes the Flather radiation condition ([Flather and Proctor, 1983](#)) for the surface elevation and depth-averaged normal velocity, Orlanski radiation conditions ([Orlanski, 1976](#)) for the tangential velocities and scalar fields, and a relaxation to the temperature and salinity from the global model near the open boundary.



Tidal forcing was provided using tidal elevation and depth-averaged normal and tangential velocities at the open boundaries from the Oregon State University (OSU) tidal data bases, which are derived from satellite altimetry data (Egbert and Erofeeva, 2003). Data from the OSU Mediterranean tidal data base were used for the K1, O1, M2, and S2 constituents and data from the OSU global data base were used for P1, Q1, K2, and N2. Tidal potential forcing for these eight constituents was used in the interior of the model domain.

Atmospheric forcing was obtained from the Coupled Ocean/Atmosphere Mesoscale Prediction System (COAMPS) (Hodur, 1997). The COAMPS setup for the Adriatic consists of a triply-nested grid with resolutions of 36, 12, and 4 km (Pullen et al., 2003). The outer grid of this nested grid system covers most of Europe and the Mediterranean and the inner 4-km grid covers the entire Adriatic and part of the Tyrrhenian Sea. COAMPS itself is nested within the Navy Operational Global Atmospheric Prediction System (NOGAPS) (Rosmond et al., 2002).

River and runoff inflows for the Adriatic were taken from the monthly climatological data base of Raicich (1994). This data base includes discharges for about 39 rivers and runoff inflows along a number of sections of the Adriatic coastline. Raicich's monthly climate values were used for all the inflows, except that daily observed discharge values were used for the Po River (Rich Signell, personal communication).

## 4. Results

### 4.1. General experimental strategy

The main experimental strategy is as follows: first, the space-dependent LSGS model (10) is tested within the framework of a purely random Eulerian velocity field that is Markovian in time. In the simplest case of zero mean flow, this model is characterized by only three parameters: the velocity variance, the correlation time, and the spatial correlation radius. For this velocity field, individual Lagrangian trajectories are described by the random-flight model (2) with a high degree of accuracy (but not exactly). Since the theory is based precisely on the Lagrangian equations of motion given by (2), it is expected that the LSGS would act to make an accurate correction toward the real trajectory properties.

Then, a much more demanding test is conducted in the context of NCOM in the Adriatic Sea, which is subject to highly-variable surface wind forcing, contains tides and surface density gradients. In addition, the three-dimensional geometry of the domain has a first-order effect on the flow field, such that there are a rich variety of co-existing turbulent flow regimes. Since, generally speaking, Eq. (2) is not an exact model for particles transported by such a complex flow field, the theory will not be strictly valid. The main idea is to explore how the LSGS method would work under such demanding circumstances.

The main experimental matrix common to both the Markov velocity field model and NCOM consists of experiments where the velocity fluctuation of the real drifters is varied in the range of  $\frac{\sigma_r}{\sigma_m} = \frac{1}{2}$ ,  $\frac{\sigma_r}{\sigma_m} = 1$ ,  $\frac{\sigma_r}{\sigma_m} = 2$ , and the correlation time is such that  $\frac{\tau_r}{\tau_m} = \frac{1}{4}$ ,  $\frac{\tau_r}{\tau_m} = 1$ ,  $\frac{\tau_r}{\tau_m} = 4$  (Table 1). To clearly identify the changes due to the LSGS correction,  $M = 121$  trajectories are released in each experiment with different initial conditions  $\boldsymbol{\eta}(0)$  for the LSGS component, and the dispersion is estimated from

$$\rho(t) = \left( \frac{1}{M} \sum_1^M (\mathbf{r}_m(t) - \mathbf{r}_m(0))^2 \right)^{1/2}. \quad (11)$$

Table 1  
The main experimental matrix

	$\frac{\sigma_r}{\sigma_m} = \frac{1}{2}$	$\frac{\sigma_r}{\sigma_m} = 1$	$\frac{\sigma_r}{\sigma_m} = 2$
$\frac{\tau_r}{\tau_m} = \frac{1}{4}$	Exp-1	Exp-2	Exp-3
$\frac{\tau_r}{\tau_m} = 1$	Exp-4	Model	Exp-5
$\frac{\tau_r}{\tau_m} = 4$	Exp-6	Exp-7	Exp-8

Since  $\rho(t) \sim \sigma\sqrt{\tau t}$ , changing  $\sigma$  and  $\tau$  by factors of two and four, respectively, should lead to comparable impacts on the trajectories. A large factor of two, rather than a subtle difference, is chosen to better illustrate the changes due to LSGS correction. Thus, eight sets of LSGS experiments are conducted (the case with  $\frac{\sigma_r}{\sigma_m} = 1$  and  $\frac{\tau_r}{\tau_m} = 1$  requires no correction).

#### 4.2. Results from the Markov velocity field model

In this section, the results are reported for a homogeneous, stationary, stochastic incompressible velocity field with zero mean and with the covariance of the stream-function given by

$$B_\psi(t, r) = 4\sigma_m^2 R^2 \exp\{-|t|/\tau_E - r^2/R^2\}, \quad (12)$$

where  $R$  is the velocity correlation radius. The values of the base parameters,  $\sigma_m = 10 \text{ cm s}^{-1}$  and  $\tau_E = 1.5$  days, are in the general range of those estimated from drifter trajectories in the Adriatic Sea (e.g., Falco et al., 2000; Poulain, 2001). However, it is not our objective to try to produce simulated trajectories that are identical to those in the Adriatic Sea. The numerical value  $R = 20$  km used in the simulations is a generic first-mode radius of deformation. The mean flow field is assumed to be zero to prevent coherent structures such as jets and recirculations from influencing the Lagrangian statistics.

The field (12) is Markovian in time. However, Lagrangian trajectories generated by it are not covered by (2) exactly. Instead, Eq. (2) yields just a very accurate description of single-particle motion because the Kubo non-linearity parameter  $K = \sigma_m \tau_E / R = 0.648$  is relatively small. Numerous experiments with different  $R$  showed that for  $K < 1$ , not only is the Lagrangian velocity well approximated by the Langevin equation, but its correlation time  $\tau_m$  is very close to the Eulerian correlation time  $\tau_E$ . For large  $K$ , this is not the case and the dependence of  $\tau_m$  on  $R$  becomes strong.

In the first series of experiments, we implemented both posterior (6) and space-dependent (10) LSGS procedures with a two-fold goal: first, to compare the two methods, and second, to check how well the real statistics are reproduced by both for the wide range of parameters given in Table 1.

Eq. (10) were solved by using the spectral decomposition of the velocity field by making use of the Markov property (see Appendix A.2). The integrations are carried out with a time step of 0.1 days for  $T = 15$  days, which is an order of magnitude larger than the correlation time scale. The first important conclusion from the 8 simulation experiments is that the estimates of the key parameters  $\tau$  and  $\sigma$  are almost the same for the posterior (6) and space-dependent (10) versions. We do not show the exact numbers, but rather state that in most cases, the difference between the parameters  $\sigma_c, \tau_c$  of the corrected velocity and the corresponding real parameters does not exceed 5%. We point out again that this result is due to small Kubo numbers (or relatively large space-correlation radii) and, in the opposite case, the divergence between the two is significant. Hence, for homogeneous environments and small Kubo numbers, the space-dependent LSGS model has the same property as the posterior procedure: it accurately reproduces the real statistics.

Let us demonstrate the changes in dispersion caused by the LSGS correction. First, spaghetti plots are shown in Fig. 4 for all 8 experiments. A total of 121 particles are released in each experiment from within a  $10 \text{ km} \times 10 \text{ km}$  area with a spacing 1 km, from which 40 trajectories are depicted. Besides the initial positions, the corrected trajectories differ among themselves by the initial conditions for the LSGS components  $\eta(0)$ . Specifically, the  $\eta(0)$ 's are sampled from the normal distribution with zero mean and variance given by (8). All the trajectories in each spaghetti diagram are obtained from the same velocity field realization (12). The diagrams clearly demonstrate the changes in the corrected trajectories caused by the changes in the real parameters.

The quantitative comparison between the targeted and achieved statistical parameters ( $\sigma, \tau$ ) in Exp-1 to Exp-8 is demonstrated in Fig. 5. This scatter plot shows that the parameters of the LSGS experiments  $\sigma_c$  and  $\tau_c$  (for definiteness: we used the estimates coming from the space-dependent version (10)) are successfully modified to change from  $(\sigma_m, \tau_m)$  toward  $(\sigma_r, \tau_r)$ . A satisfactory agreement is obtained in all the experiments, even though in some cases, as in Exp. 1, the relative error can reach 30–40%. We suggest that a significant difference between  $\sigma_c$  and  $\sigma_r$  in this case could be caused by the combination of two factors: first, the sample variability of the statistical estimate of the corrected velocity and, second, imperfect performance of the LSGS correction. Even though the total sample size  $N = 121 \times 150 = 18,150$  looks impressive, the equivalent number of independent observations,  $N_e$ , is much smaller. Indeed, for each trajectory,  $N_e = 15/\tau_r$  is only 40 and

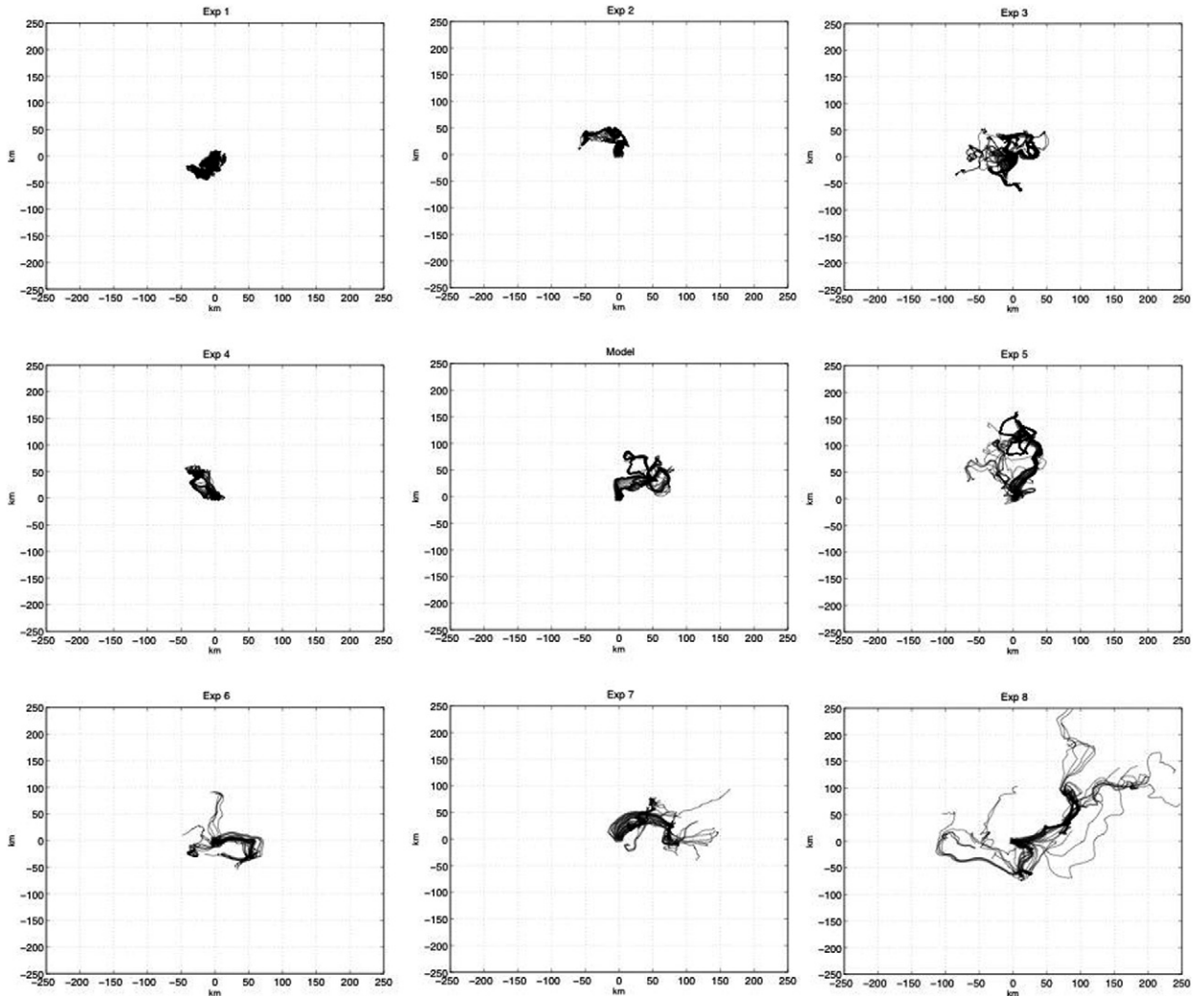


Fig. 4. Fifteen-day long trajectories of 121 particles for Exp-1 to Exp-8 and Set-A generated by the random field model using the space-dependent version of the LSGS model. Red and blue points mark the initial and final positions, respectively. The model run (without LSGS) is depicted in the middle panel.

the trajectories in each cluster are strongly dependent since they start close to one another, which probably makes total  $N_c$  two orders of magnitude less than  $N$ . As for the correction method itself, recall that the theory presented in Section 2 is exact for the posterior version only and it is essentially based on continuous time consideration, stationarity, and Gaussianity. In experiments, the first condition cannot be fulfilled while the others hold only approximately. It is not surprising that superposition of all the listed factors can sometimes affect results, even though the effect of each one of them seems negligible.

The plots of  $\rho(t)$  defined in (11) and those obtained from the basic model (2) with the real parameters

$$\rho_r(t) = 2\sigma_r(\tau_r(t - \tau_r(1 - \exp(-t/\tau_r))))^{1/2}$$

are shown in Fig. 6 for a subset of experiments, namely for Exps. 3, 4, and 7. Each of these experiments is taken from a different column and row of Table 1 to better represent the whole variety of relations between the model and real parameters. The model curve  $\rho_m(t)$  of the same analytical form as the model parameters is also plotted. For Exps. 3 and 4, the agreement between the curves is very good in both the initial and final stages. For Exp. 7 that difference is significant. Even though the corrected and real parameters in this

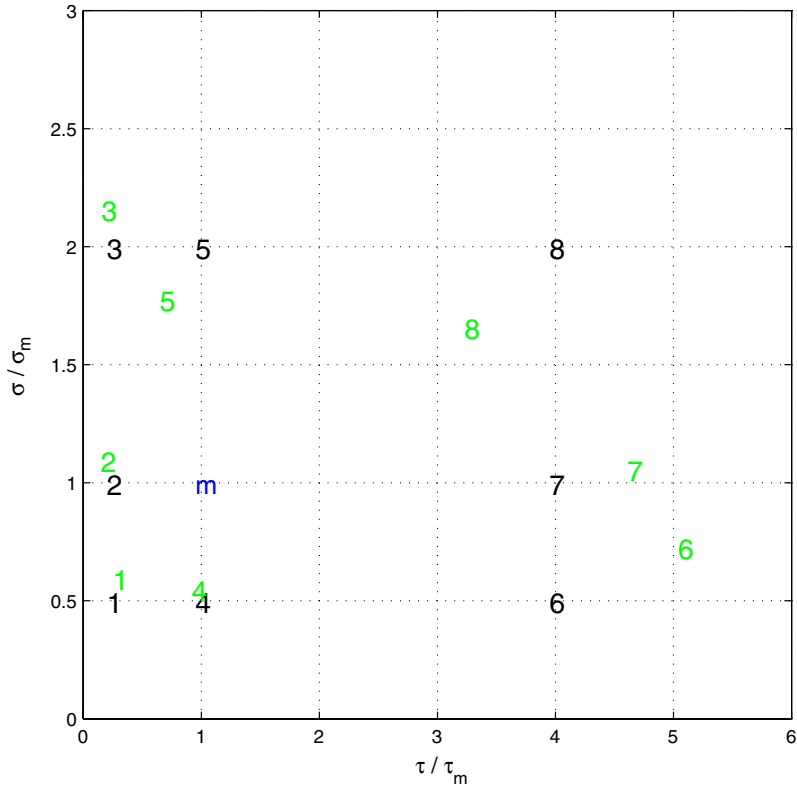


Fig. 5. Scatter plot of targeted and achieved values of the statistical parameters from real and corrected particle trajectories in experiments shown in Fig. 4. The numbers in black denote experiments (Table 1) at locations  $(\frac{\sigma_r}{\sigma_m}, \frac{\tau_r}{\tau_m})$ , while numbers in green mark  $(\frac{\sigma_c}{\sigma_m}, \frac{\tau_c}{\tau_m})$ . The model parameters are marked by the symbol “m”.

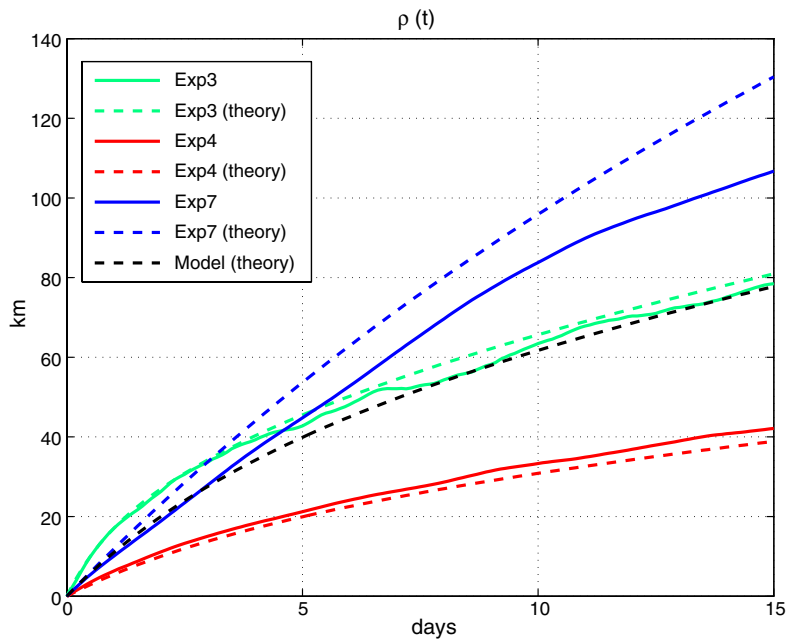


Fig. 6. Time evolutions of  $\rho(t)$  from the random field model (solid lines) and  $\rho_r(t)$  (dashed lines) for selected experiments.

experiment are closer than those in Exps. 3 and 4, the divergence at the 15th day is essentially larger because of the different behavior during the initial stage. In Exps. 6 and 8, the gap between the corrected and real variances is larger than those in Exps. 3, 4, and 7 and the relative differences between  $\rho(15)$  and  $\rho_r(15)$  are 20% and 27%, respectively. In summary, the method not only gives rise to the real parameters, but is also able to reproduce the whole time evolution of the dispersion curve satisfactorily.

#### 4.3. Application to NCOM in the Adriatic Sea

The mean surface flow field from the NCOM simulation is depicted in Fig. 7a. The reader is referred to Poulain (1999, 2001), Cushman-Roisin et al. (2001), Falco et al. (2000) and Maurizi et al. (2004) for a comprehensive discussion of the circulation features and data sets. The main point is that the NCOM simulation employed here adequately approximates the main features of the circulation.

Two release locations are chosen (Fig. 7b) away from coastal regions to avoid for as long as possible the flow regime change that can be induced by the strong boundary currents characteristic of the circulation field. These mid-basin regions in the southern and northern parts of the Adriatic domain are square in shape with sides of length 30.6 km, in which 121 drifters are launched in a Cartesian array. The domain size was also chosen for an adequate coverage to evaluate the decorrelation timescales and the rms velocity fluctuations of both the model and corrected trajectories. Since the flow is highly variable, two different release periods, October 2–17 and October 12–27, 2002, are considered in addition to the different locations. The parameters

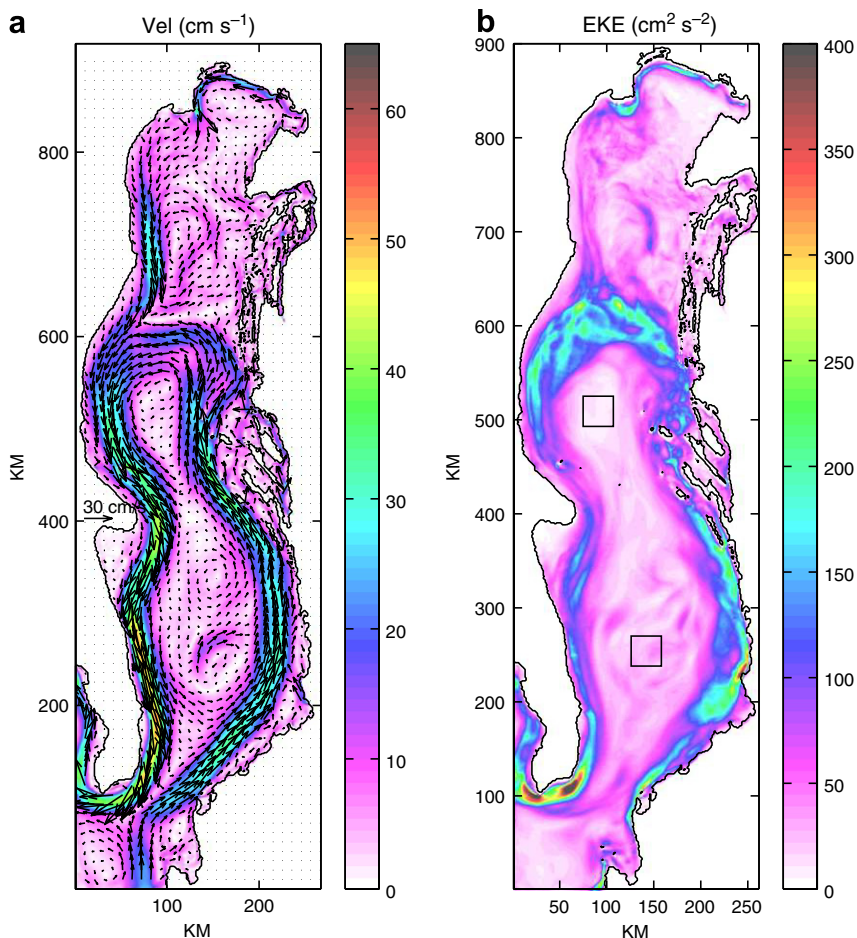


Fig. 7. (a) Surface mean flow and (b) the eddy kinetic energy distribution and the two drifter launch areas in NCOM.

Table 2

Parameters of modeled trajectories released in two different locations and two different periods in NCOM

	Location: south middle basin	Location: north middle basin
Period: October 2–17, 2002	Set-A: $\sigma_m^u = 5.7 \text{ cm s}^{-1}$ ; $\sigma_m^v = 4.2 \text{ cm s}^{-1}$ $\tau_m^u = 2.1 \text{ days}$ ; $\tau_m^v = 1.7 \text{ days}$	Set-C: $\sigma_m^u = 3.8 \text{ cm s}^{-1}$ ; $\sigma_m^v = 2.5 \text{ cm s}^{-1}$ $\tau_m^u = 1.3 \text{ days}$ ; $\tau_m^v = 1.5 \text{ days}$
Period: October 12–27, 2002	Set-B: $\sigma_m^u = 5.3 \text{ cm s}^{-1}$ ; $\sigma_m^v = 4.7 \text{ cm s}^{-1}$ $\tau_m^u = 1.5 \text{ days}$ ; $\tau_m^v = 2.9 \text{ days}$	Set-D: $\sigma_m^u = 4.3 \text{ cm s}^{-1}$ ; $\sigma_m^v = 2.9 \text{ cm s}^{-1}$ $\tau_m^u = 1.3 \text{ days}$ ; $\tau_m^v = 1.0 \text{ days}$

of the model trajectories estimated from these releases are summarized in Table 2. First, we observe that there is a significant anisotropy in the parameters, and second, they exhibit quite a bit of variation in time and space, thus providing a total of four test beds, denoted Set-A to Set-D, to explore the performance of the LSGS model. The experiments with the LSGS model are carried out for the main experimental matrix (Table 1) in each of the four test beds (Table 2), on the basis of 121 drifters, each initiated with 10 different  $\eta(0)$  realizations according to the  $\eta$  variance defined by Eq. (8) in Section 2 (namely, a total of  $8 \times 4 \times 12 \times 10 = 38,720$  synthetic drifters). The NCOM velocity fields have been low-pass filtered using a 1.5-day window in order to remove high-frequency motions, such as the inertial oscillations strongly present in the interior gyres.

Trajectories of particles released in Set-A (Table 2) are shown for Exp-1 to Exp-8 in Fig. 8. Certain symmetries are clearly apparent from a visual inspection of the trajectories. There is not a significant difference between the trajectories obtained in Exp-3, Exp-6, and the model, while those from Exp-4 and Exp-2 (Exp-5 and Exp-7) exhibit somewhat less (more) dispersion with respect to the initial launch positions, and the dispersion in Exp-1 (Exp-8) is significantly less (more) than is the case with the original model. Qualitatively similar and consistent behavior is seen for the case of Set-D (Fig. 9) and the other two sets (Sets-B and C, not shown). The preliminary conclusion from these plots is that the LSGS model has a significant effect on the particle trajectories that is consistent with the behavior expected from the modification of  $\sigma$  and  $\tau$  in Exp-1 to Exp-8. In particular, we note that the LSGS model acts successfully not only to enhance the particle dispersion, but also to reduce it.

The accuracy of the LSGS model in modifying the particle transport as specified is explored using the scatter plots of the targeted  $(\frac{\sigma_r}{\sigma_m}, \frac{\tau_r}{\tau_m})$  and achieved  $(\frac{\sigma_c}{\sigma_m}, \frac{\tau_c}{\tau_m})$  parameters for Exp-1 to Exp-8. Since there are four sets of experiments in NCOM, parameters  $(\sigma_c, \tau_c)$  averaged over all Sets A to D are shown. The agreement between  $(\sigma_c, \tau_c)$  and  $(\sigma_r, \tau_r)$  is satisfactory in both the zonal and meridional directions and for all experiments (Fig. 10).

Quantitative results for the dispersion of the particles with respect to the initial launch location  $\rho(t)$  are shown in Fig. 11. Based on the formula given in Piterbarg (2001a), one would expect  $\rho_r(t)/\rho_m(t) \approx \sigma_r \sqrt{\tau_r}/(\sigma_m \sqrt{\tau_m})$  in the so-called inertial regime for large  $t$ . This corresponds to a factor of  $\frac{1}{4}$  for Exp-1,  $\frac{1}{2}$  for Exp-2 and Exp-4, 1 for Exp-3 and Exp-6, 2 for Exp-5 and Exp-7, and 4 for Exp-8. This asymptotic estimate is subject to the assumption of large  $t$ , isotropy, and homogeneity, which are not strictly valid in the case of the NCOM simulations, but provide a scale for the differences in dispersion that should be anticipated. In light of these estimates, the results illustrated in Fig. 11 appear to be reasonably consistent and quite encouraging, in particular given the complexity of the flow field regulated by the geometry, forcing fields, and internal dynamics.

In light of these systematic experiments, which appear to show that the LSGS model accurately corrects the correlation time scales and turbulent velocity fluctuations, further experiments are conducted with realistic values observed in the Adriatic circulation. A number of studies have been conducted to analyze the large drifter data set collected by P.M. Poulain in the Adriatic Sea (Poulain, 1999, 2001; Falco et al., 2000; and Maurizi et al., 2004). The circulation is generally divided into dynamically-different regions in space, such as the western Adriatic current and interior gyres, and different seasons in time, and the estimated values for  $\sigma_r$  and  $\tau_r$  exhibit a broad range. Here, we will work with the bulk estimates based on Falco et al. (2000) for the interior gyres, namely  $\sigma_r^u \approx \sigma_r^v \approx 10 \text{ cm s}^{-1}$  and  $\tau_r^u \approx \tau_r^v \approx 2 \text{ days}$ . Two sets are chosen, one in the south and the other in the north, namely Set-A and Set-C (Table 2). Therefore, for Set-A,  $\frac{\sigma_r^u}{\sigma_m^u} = 1.75$ ,  $\frac{\sigma_r^v}{\sigma_m^v} = 2.38$ ,  $\frac{\tau_r^u}{\tau_m^u} = 1.05$ ,  $\frac{\tau_r^v}{\tau_m^v} = 0.85$ ,

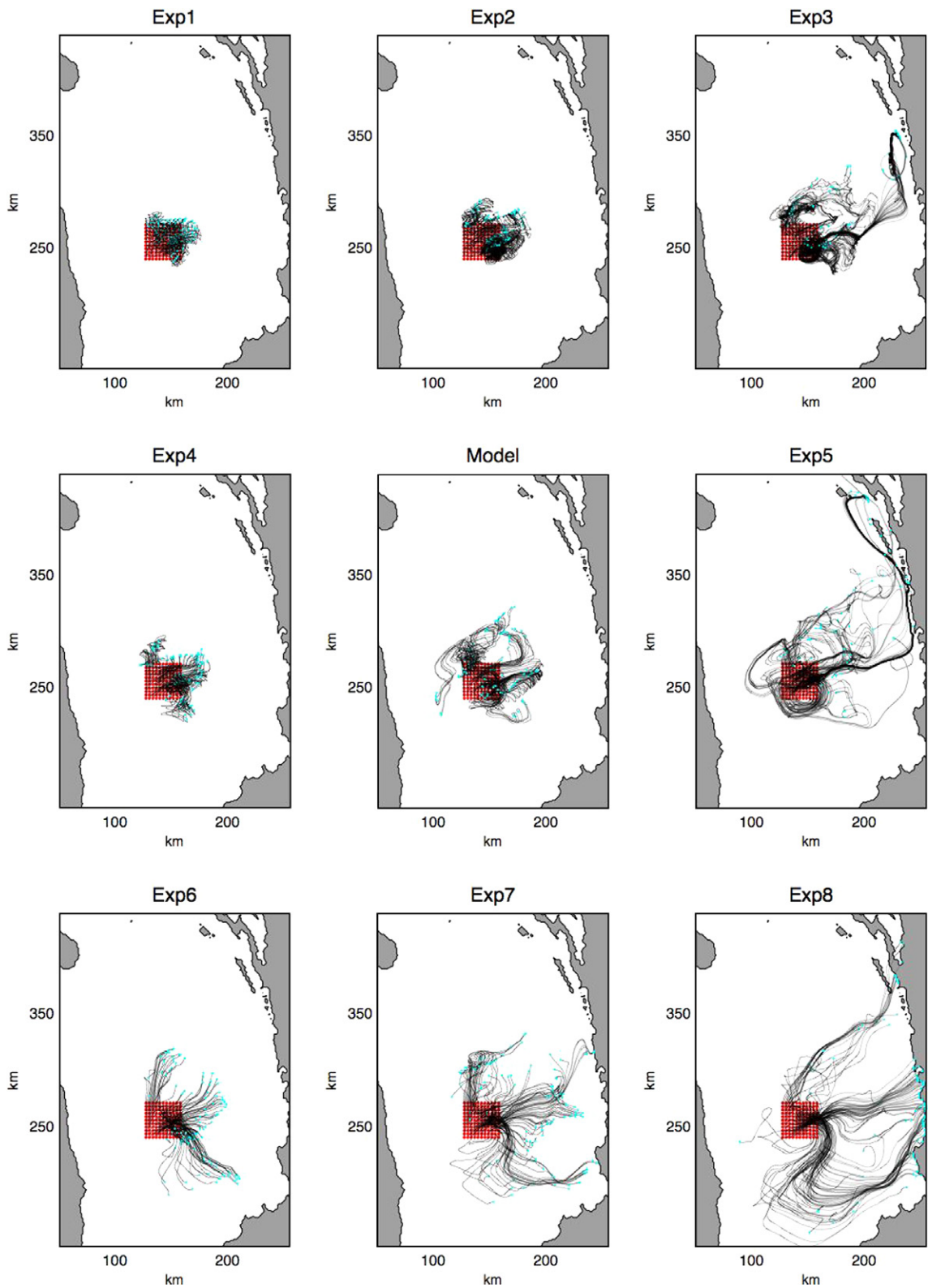


Fig. 8. Fifteen-day long trajectories of 121 particles for Exp-1 to Exp-8 and Set-A in NCOM (only 1  $\eta(0)$  displayed). Red and blue points mark the initial and final positions, respectively. The model run (without LSGS) is depicted in the middle panel.

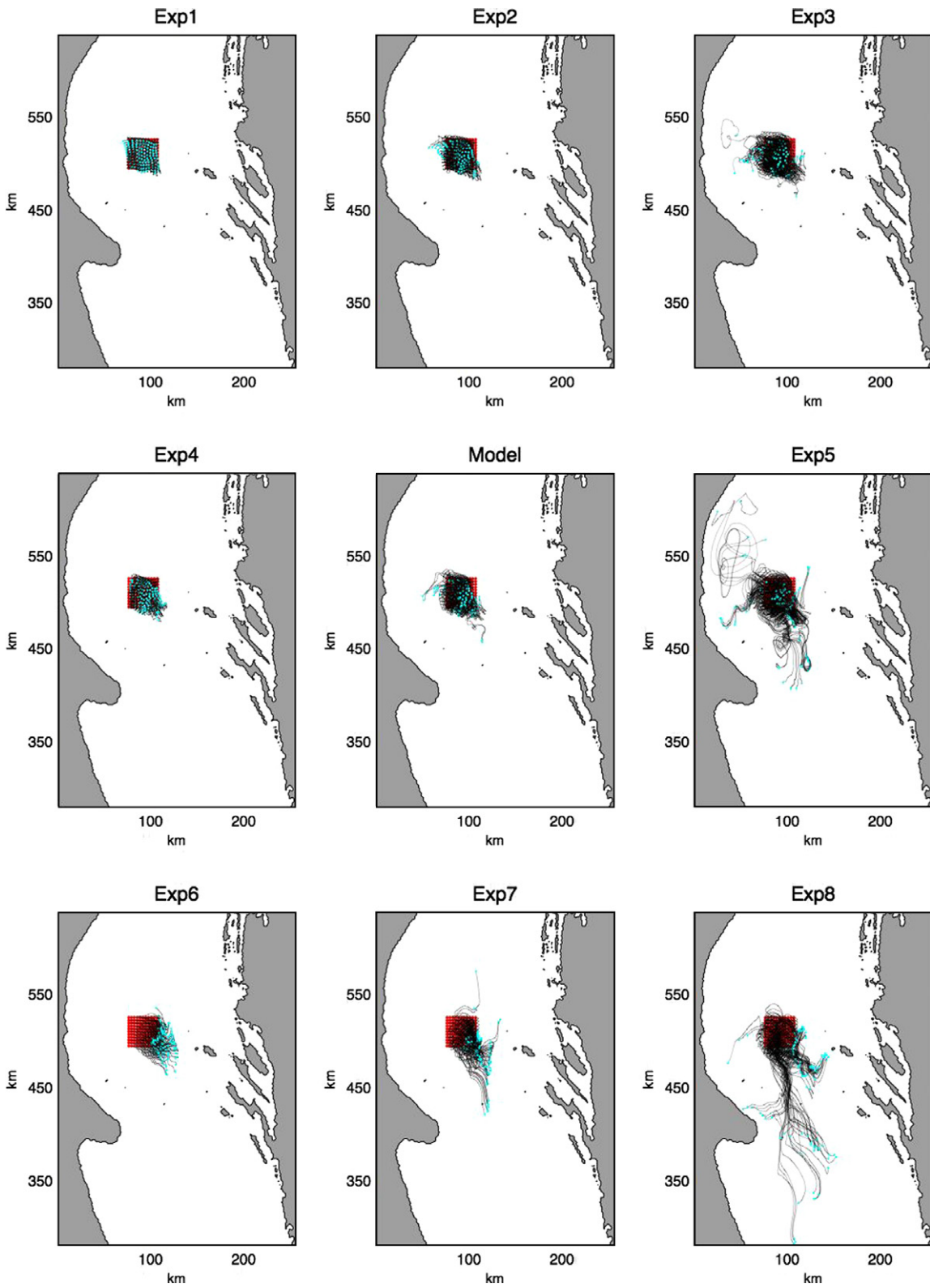


Fig. 9. Same as Fig. 4, but for Set-D.



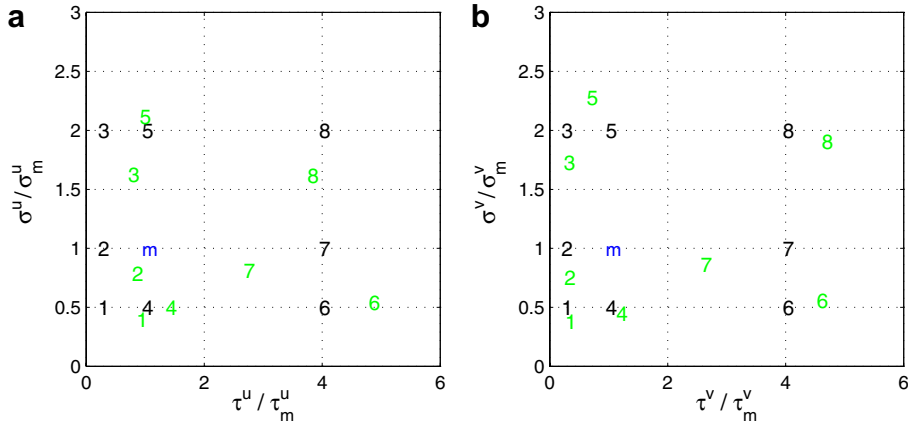


Fig. 10. Scatter plot of the targeted  $(\frac{\sigma_c}{\sigma_m}, \frac{\tau_c}{\tau_m})$  and achieved  $(\frac{\sigma_a}{\sigma_m}, \frac{\tau_a}{\tau_m})$  parameters for Exp-1 to Exp-8 calculated from particles released in NCOM, and averaged over Sets A to D in (a) zonal and (b) meridional directions.

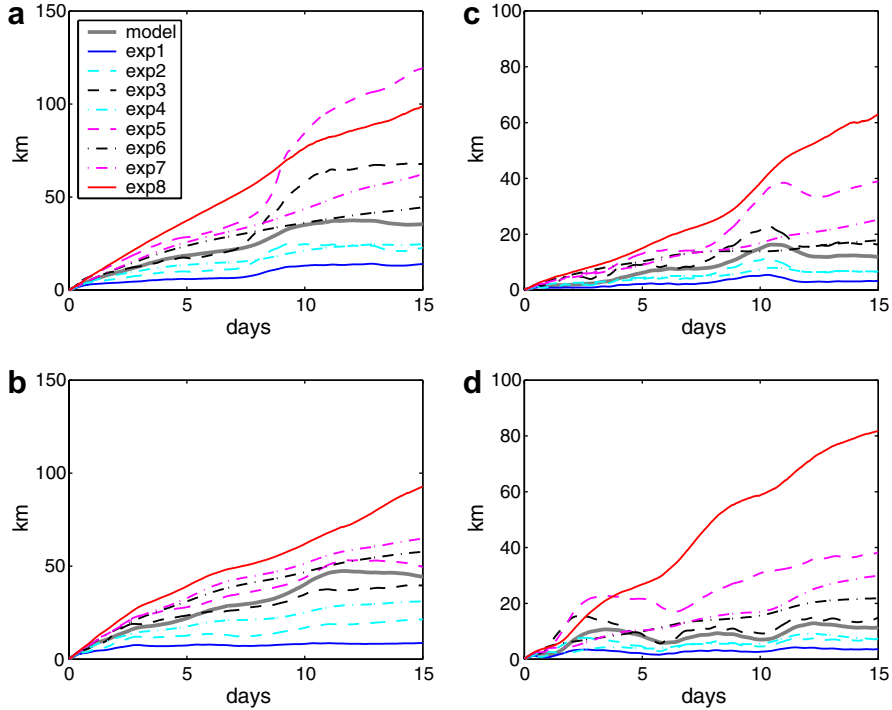


Fig. 11. Dispersion with respect to the launch locations,  $\rho(t)$ , for Exp-1 to Exp-8 in: (a) Set-A; (b) Set-B; (c) Set-C and (d) Set-D in NCOM.

and for Set-C,  $\frac{\sigma^u}{\sigma_m^u} = 2.63$ ,  $\frac{\sigma^v}{\sigma_m^v} = 4.0$ ,  $\frac{\tau^u}{\tau_m^u} = 1.53$ ,  $\frac{\tau^v}{\tau_m^v} = 1.33$ . Thus, the correlation time scale appears to be quite accurate in NCOM, whereas the turbulent velocity fluctuations are somewhat underestimated, which can be due to the many different factors discussed in Section 1. A factor of two in either the velocity fluctuation or time scale seems to be a typical size of the error encountered in realistic numerical models (e.g., Garraffo et al., 2001). It should also be noted that the data can contain errors due to subsampling in time along the trajectories and/or lack of data representative of the exact simulation period. In any case, our primary purpose is to provide a feel of the typical corrections by the LSGS model to the modeled particle trajectories.

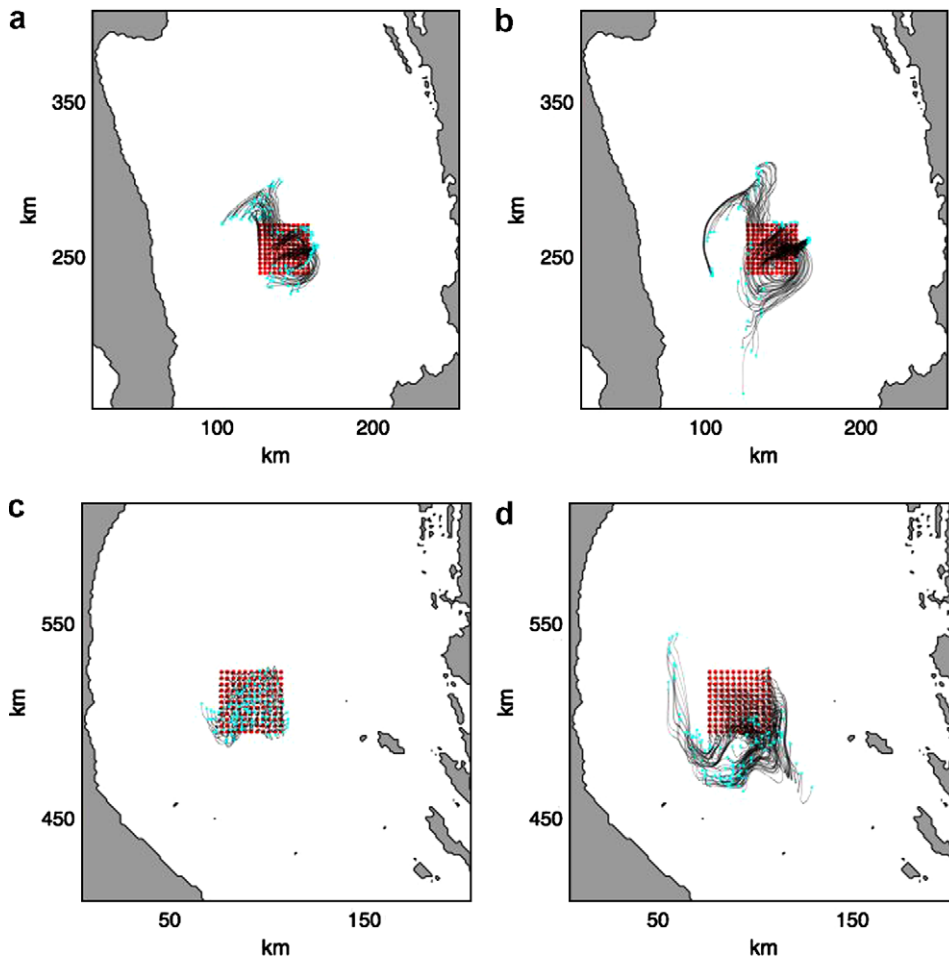


Fig. 12. Comparison of 7-day trajectories from NCOM without (left panels) and with (right panels) the LSGS model for Set-A (top panels) and Set-C (bottom panels). The mean flow is not included in the particle advection. (a) Model – Set-A; (b) LSGS – Set A; (c) Model – Set C; (d) LSGS – Set C.

Comparison of 7-day trajectories with and without the LSGS model are shown in Fig. 12. As expected by the ratios of  $\sigma_r/\sigma_m$ , the contribution of the LSGS model to the transport of the particles is rather significant in that they travel much longer distances, even though the initial part of the trajectories does not appear too different.

Finally, the mean flow is added in order to advect the particles with the full field. The results (Fig. 13) still indicate a significant difference in those cases with the LSGS model. Since the regions are chosen to coincide with a small ratio of mean and eddy kinetic energy, this result is to be expected. The contribution of the LSGS model in other regions, such as the western Adriatic current, is likely to be relatively smaller.

## 5. Summary and conclusions

An accurate calculation of the Lagrangian transport is important for a number of practical problems, such as dispersion of pollutants, biological species, and sediments. Precise techniques to characterize the Lagrangian pathways have been developed in the context of dynamical system theory, but they rely on the accuracy of the Eulerian velocity fields, which are typically derived from ocean and coastal models. Yet, these models not only contain a series of errors due to uncertainties in the forcing and boundary conditions, model physics, and unresolved space and time scales, but they are also very expensive as they are typically run with the highest

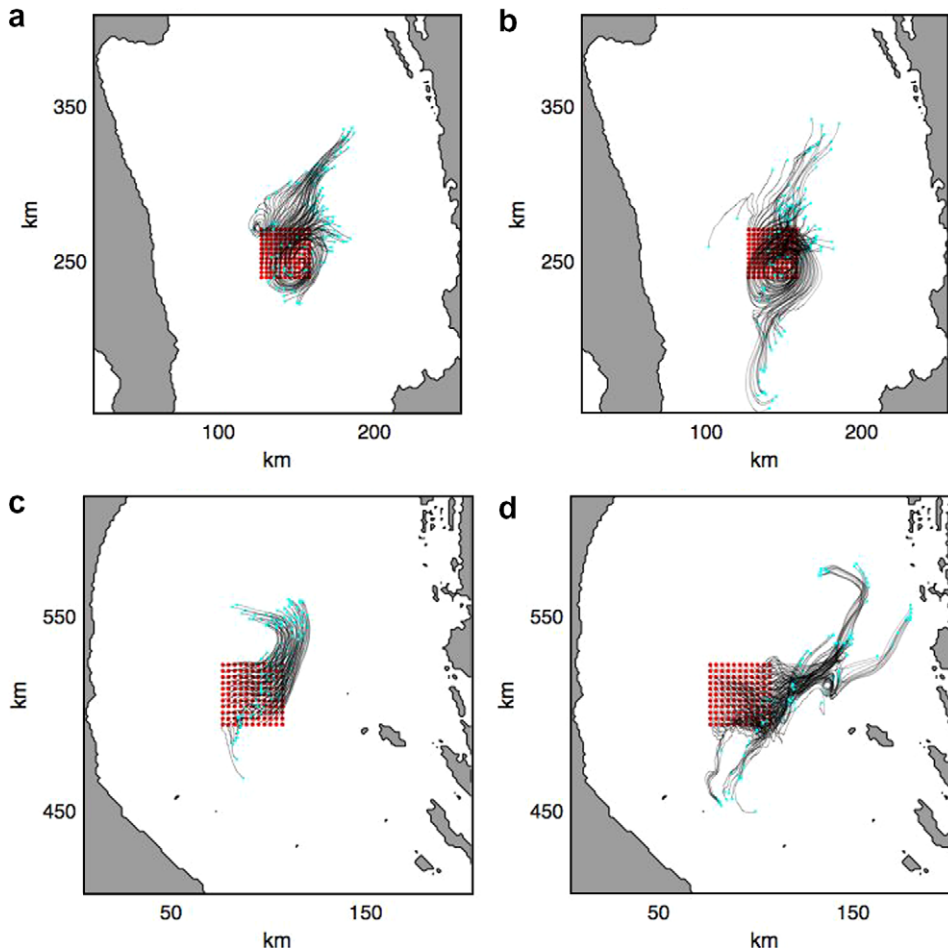


Fig. 13. Same as Fig. 9 but with the mean flow field included in particle advection. (a) Model – Set A; (b) LSGS – Set A; (c) Model – Set C; (d) LSGS – Set C.

resolution permitted by the available computational resources. In particular, an ensemble of experiments is desirable to determine model uncertainty, but remains prohibitive, since the combinative number and range of the parameters that affect the Eulerian field can be very large. Therefore, the problem arises of how to remove or reduce the errors that propagate from the Eulerian field to the Lagrangian transport.

In this study, a simple and practical method is developed in order to reduce the errors in the Lagrangian transport, given the time evolution of a velocity field. The main concept is to employ the statistical behavior of particle trajectories from observational data sets. The so-called LSGS method is developed, which supplies a correctional velocity vector  $\eta(t)$  in the Lagrangian transport equation to reduce the discrepancy of statistical parameters, namely the correlation time scale and turbulent velocity fluctuation, between model-generated ( $\tau_m, \sigma_m$ ) and observed ( $\tau_r, \sigma_r$ ) trajectories, such that the corrected particle trajectories show behavior similar to the observed ones ( $\tau_c \approx \tau_r, \sigma_c \approx \sigma_r$ ).

The LSGS method is derived theoretically in the context of a random-flight model, in which trajectories with parameters  $\tau$  and  $\sigma$  are simulated directly, namely without the need of an underlying Eulerian velocity field. Then, a space-dependent version of the LSGS method is derived using the so-called Markov velocity field model, in which stochastic velocity fields are generated as an idealized representation of two-dimensional, homogenous, stationary, turbulent flows. The LSGS model is tested in the context of the Markov velocity field model to investigate its performance in reproducing  $\tau_c \approx \tau_r$  and  $\sigma_c \approx \sigma_r$  using a series of experiments with different ratios of  $\frac{\tau_r}{\tau_m}$  and  $\frac{\sigma_r}{\sigma_m}$ . It is shown that satisfactorily accurate results are obtained.

The same series of experiments are then conducted based on the hourly output from a realistic ocean model, the Navy Coastal Ocean Model, configured for the Adriatic Sea with high spatial (1-km) resolution. The model is subject to realistic forcing from (4-km COAMPS) winds, tides, and river runoff, and coupled to a coarser resolution global model. Two regions are selected with a high ratio of eddy to mean kinetic energy to maximize the effect of turbulent fluctuations on the dispersion of particles (rather than dispersion by the mean shear) and away from the boundaries, where the flow parameters change and become strongly anisotropic. Despite the general complexity of the flow patterns, reasonably good results are obtained using the LSGS. Finally, a set of experiments including the mean flow and realistic  $\tau_r$  and  $\sigma_r$  for these regions demonstrate that the effect of the LSGS method on the particle trajectories seems significant, despite the realistic forcing and realistic model circulation. Given the difficulty of capturing exactly the turbulent fields, the use of such LSGS models in particle transport routines in OGCMs appears to be a necessary and promising avenue.

The LSGS method offers three significant advantages. First, it can be applied in principle to models at all resolutions. Since OGCMs use dissipative eddy-viscosity Laplacian operators, the effect of turbulent flows at the subgrid scale is suppressed. But given that oceanic drifters feel forces at their own physical scale, the accuracy of particle dispersion by turbulent fluctuations reduces with increasing grid spacing. For instance, the LSGS model could be particularly suitable for large-scale OGCMs, in which the tendency of  $\tau_m < \tau_r$  and  $\sigma_m < \sigma_r$  is encountered (Garraffo et al., 2001). Second, LSGS models can act not only to enhance  $\tau_m$  and  $\sigma_m$  but also to reduce them, if necessary, from the observations. Finally, LSGS models can be applied off-line using the archived model output and there is no need to rerun the OGCM. In addition, the calculation of  $\eta(t)$  is not a computationally expensive procedure. The primary requirement for the LSGS method is that observational drifter data sets with sufficient coverage are needed to determine  $\tau_r$  and  $\sigma_r$  in the region of interest.

The limitations of the LSGS method also need to be clarified. The present LSGS method corrects turbulent velocity components only. Thus, corrections are likely to be more effective in regions where the turbulent component is significant with respect to the mean velocity component. This is because of our assumption that the turbulent component of the ocean flow field is usually much more difficult to reproduce in numerical models than the mean circulation. Nevertheless, if the mean currents are incorrect in boundary currents and various frontal zones, the present LSGS method is not likely to be very helpful. The exact locations of so-called hyperbolic points associated with the mean field can also have a determining impact on particle dispersion. Thus, this method is aimed primarily to fine-tune the Lagrangian transport from an accurate numerical model of the circulation being investigated, under the practical assumption that the exact reproduction of the turbulent flow field can be a very cumbersome effort because of many delicate processes that need to be resolved (Section 1) while it is generally easier to improve the computation of the mean fields.

Several avenues will be pursued in future studies. First,  $\tau_r$  and  $\sigma_r$  do not usually remain constant as particles travel with the flow field. Therefore, incorporation of varying  $\frac{\tau_r}{\tau_m}$  and  $\frac{\sigma_r}{\sigma_m}$  along the particle trajectories needs to be considered, particularly for semi-enclosed seas, such as the Adriatic Sea, that are characterized by strong boundary currents. Second, the LSGS method can be used in the calculation of the Lagrangian structures, for instance, from the local finite scale Lyapunov exponent (FSLE, Aurell et al., 1997; Artale et al., 1997).

## Acknowledgements

The authors greatly appreciate the support of ONR via Grants N00014-05-1-0094 and N00014-05-1-0095 (A. Haza, A. Griffa and T. Özgökmen) and N00014-99-0042 (L. Piterbarg) and via the Dynamics of the Adriatic in Real-Time (DART) Project under Program Element Number 0602435N (P. Martin). We also thank Michel Rixen for stimulating study of this problem.

## Appendix A

### A.1. Proof of LSGS model formula (5)

Consider the stationary solution  $\eta$  of (5) and proof that the spectral tensor of  $\mathbf{v}_c$  defined in (4) coincides with that of  $\mathbf{v}_r$ . Since both have zero mean, that would imply statistical equivalence of  $\mathbf{v}_c$  and  $\mathbf{v}_r$ .

First, notice the following expression for the spectral tensors of real velocity

$$E_r(\omega) = \frac{1}{2\pi} A_r B_r(\omega)^{-1} A_r, \quad B_r(\omega) = \omega^2 I + A_r A_r^* - i\omega(A_r - A_r^*), \quad (\text{A.1})$$

where the star means complex conjugate and a similar expression for the model tensor  $E_m$  with replacing  $A_r$  and  $A_r$  by  $A_m$  and  $A_m$ , respectively. Matrix  $B_r$  allows factorization

$$B_r = C_r C_r^*, \quad C_r(i\omega) = \begin{pmatrix} 1/\tau_{r,u} + i\omega & \Omega \\ -\Omega & 1/\tau_{r,v} + i\omega \end{pmatrix} \quad (\text{A.2})$$

and similar factorization is valid for

$$B_m = C_m C_m^*. \quad (\text{A.3})$$

Obviously

$$Q(x) = A_r C_r^*(x) A_r^{-1}, \quad P = A_r C_m^*(x) A_m^{-1} - A_r C_r^*(x) A_r^{-1}. \quad (\text{A.4})$$

To verify that  $\mathbf{v}_c$  and  $\mathbf{v}_r$  have the same spectrum, it is sufficient to check the relation

$$Q(i\omega) E_r(i\omega) Q(i\omega)^* = P(i\omega) E_r(i\omega) P(i\omega)^*.$$

That can be done straightforwardly by substituting expressions (A.1)–(A.4) into the last relation.

The following formula for the spectral density of  $\eta$  follows from (6)

$$E_\eta(\omega) = \frac{a^2 \omega^2 + b^2}{c^2 + \omega^2} \frac{\tau_m \sigma_m^2}{\pi(1 + \tau_m^2 \omega^2)}$$

By integrating this expression in  $\Omega$  one obtains

$$\overline{\eta^2} = \frac{(\tau_m b^2 - ca^2) \sigma_m^2}{c(c\tau_m - 1)}$$

which becomes (8) after accounting for (7). Next by multiplying (6) consequently by  $\eta$  and  $u'_m$  and averaging we get for covariance  $R_{m\eta} = \overline{u'_m \eta}$

$$R_{m\eta} = \frac{c\overline{\eta^2} - ab\sigma_m^2}{ac - b}$$

Using the last two expressions one can easily find the correlation coefficient  $r_{cm}$  which is reduced to the formula in the main text after some algebra.

## A.2. Markov velocity field model algorithm

The velocity field with stream-function covariance (12) can be obtained as a solution of the equation

$$\frac{\partial \Psi}{\partial t} + \Psi/\tau = \Phi(t, x, y) \quad (\text{A.5})$$

driven by a Gaussian white-noise forcing with covariance

$$E\Phi(t_1, x_1, y_1)\Phi(t_1 + t, x_1 + x, y_1 + y) = 8\sigma_m^2 R^2 \tau_m^{-1} \delta(t) \exp(-r^2/R^2).$$

The forcing in (A.5) is taken as

$$\Phi(t, x, y) = \sum_{k_1, k_2=-K}^K \sigma(\mathbf{k}) (\zeta_{\mathbf{k}}(t) \sin \phi + \eta_{\mathbf{k}}(t) \cos \phi), \quad \mathbf{k} = (k_1, k_2), \quad \phi = k_1 x + k_2 y, \quad (\text{A.6})$$

where  $\mathbf{k}$  is a wave vector,  $(2K + 1)^2$  is the total number of harmonics,  $\zeta_{\mathbf{k}}(t), \eta_{\mathbf{k}}(t)$  are independent white noises in both  $t$  and  $\mathbf{k}$ , and finally  $\sigma(\mathbf{k})$  is an amplitude that in our experiments was taken as

$$\sigma^2(\mathbf{k}) = A^2 \exp(-sk^2),$$

where parameters  $A, s > 0$  are related to  $\sigma_m, R, \tau_m$  by

$$A = \frac{4R^2\sigma_m}{\sqrt{\pi\tau_m}}, \quad s = \left(\frac{\pi R}{2K}\right)^2.$$

Thus, we consider a zero mean flow with no spin ( $\omega = 0$ ) excited by a finite number of random harmonics. From (A.6) it follows that the velocity field satisfies

$$\frac{\partial \mathbf{u}}{\partial t} = -A\mathbf{u} + \mathbf{f}(t, \mathbf{x}) \quad (\text{A.7})$$

with forcing components along  $x$ - and  $y$ -axes, respectively, given by

$$f_x = \sum_{\mathbf{k} \in K} k_2 \sigma(\mathbf{k}) Q_{\mathbf{k}}(t, x, y), \quad f_y = - \sum_{\mathbf{k} \in K} k_1 \sigma(\mathbf{k}) Q_{\mathbf{k}}(t, x, y), \quad Q_{\mathbf{k}} = \zeta_{\mathbf{k}}(t) \cos \phi - \eta_{\mathbf{k}}(t) \sin \phi.$$

Introduce stochastic processes  $p_{\mathbf{k}}(t), q_{\mathbf{k}}(t)$  satisfying

$$dp_{\mathbf{k}}(t)/dt + p_{\mathbf{k}}(t)/\tau = \zeta_{\mathbf{k}}(t), \quad dq_{\mathbf{k}}(t)/dt + q_{\mathbf{k}}(t)/\tau = \eta_{\mathbf{k}}(t). \quad (\text{A.8})$$

Then the components of the Eulerian velocity field are given by

$$u_x = \sum_{\mathbf{k} \in K} k_2 \sigma(\mathbf{k}) (p_{\mathbf{k}}(t) \cos \phi - q_{\mathbf{k}}(t) \sin \phi), \quad u_y = - \sum_{\mathbf{k} \in K} k_1 \sigma(\mathbf{k}) (p_{\mathbf{k}}(t) \cos \phi - q_{\mathbf{k}}(t) \sin \phi) \quad (\text{A.9})$$

as follows from (A.7). For the Lagrangian velocity we have

$$\begin{aligned} dv_x/dt &= \partial u_x / \partial t + v_x \partial u_x / \partial x + v_y \partial v_x / \partial y |_{x=x(t), y=y(t)}, \\ dv_y/dt &= \partial u_y / \partial t + v_x \partial u_y / \partial x + v_y \partial u_y / \partial y |_{x=x(t), y=y(t)}. \end{aligned} \quad (\text{A.10})$$

Finally, from (A.10) we get

$$dv_x/dt = v_x(-1/\tau + E_{11}(p_{\mathbf{k}}, q_{\mathbf{k}})) + v_y E_{12}(p_{\mathbf{k}}, q_{\mathbf{k}}), \quad dv_y/dt = v_y(-1/\tau + E_{21}(p_{\mathbf{k}}, q_{\mathbf{k}})) + v_x E_{22}(p_{\mathbf{k}}, q_{\mathbf{k}}), \quad (\text{A.11})$$

where

$$E_{11} = \sum_{\mathbf{k} \in K} k_1 k_2 \sigma(\mathbf{k}) \widetilde{Q}_{\mathbf{k}}, \quad E_{12} = - \sum_{\mathbf{k} \in K} k_2^2 \sigma(\mathbf{k}) \widetilde{Q}_{\mathbf{k}}, \quad E_{21} = \sum_{\mathbf{k} \in K} k_1^2 \sigma(\mathbf{k}) \widetilde{Q}_{\mathbf{k}}, \quad E_{22} = -E_{11}$$

and

$$\widetilde{Q}_{\mathbf{k}} = -\zeta_{\mathbf{k}}(t) \sin \phi - \eta_{\mathbf{k}}(t) \cos \phi.$$

Formula (A.11) for the zonal and meridional components of the Lagrangian velocity is used to generate the trajectories of particles driven by the stream function  $\Psi$ .

## References

- Artale, V., Boffetta, G., Celani, A., Cencini, M., Vulpiani, A., 1997. Dispersion of passive tracers in closed basins: beyond the diffusion coefficient. *Phys. Fluids* 9, 3162–3171.
- Aurell, E., Boffetta, G., Crisanti, A., Paladin, G., Vulpiani, A., 1997. Predictability in the large: an extension of the concept of Lyapunov exponent. *J. Phys. A* 30, 126.
- Barron, C.N., Kara, A.B., Hurlburt, H.E., Rowley, C., Smedstad, L.F., 2004. Sea surface height predictions from the global navy coastal ocean model (NCOM) during 1998–2001. *J. Atmos. Ocean. Technol.* 21 (12), 1876–1894.
- Barron, C.N., Kara, A.B., Martin, P.J., Rhodes, R.C., Smedstad, L.F., 2006. Formulation, implementation and examination of vertical coordinate choices in the global Navy Coastal Ocean Model (NCOM). *Ocean Modell.* doi:10.1016/j.ocemod.2005.01.004.
- Bauer, S., Swenson, M., Griffa, A., 2003. Eddy mean flow decomposition and eddy diffusivity estimates in the Tropical Pacific Ocean: 2 results. *J. Geo. Res.* 107, 3154.
- Berloff, P., McWilliams, J.C., 2002. Material transport in Oceanic gyres. Part 2: Hierarchy of stochastic models. *J. Phys. Oceanogr.* 32 (3), 797–830.
- Blumberg, A.F., Mellor, G.L., 1987. A description of a three-dimensional coastal ocean circulation model. In: Heaps, N. (Ed.), *Three-Dimensional Coastal Ocean Models*. American Geophysical Union, New York, NY, p. 208.

- Borgas, M.S., Flesch, T.K., Sawford, B.L., 1997. Turbulent dispersion with broken reflectional symmetry. *J. Fluid Mech.* 279, 6999.
- Caglar, M., Özgökmen, T.M., Piterbarg, L.I., 2006. Parameterization of submeso-scale eddy-rich flows using a stochastic velocity model. *J. Ocean. Atmos. Technol.* 23 (12), 1745–1758.
- Castellari, S., Griffa, A., Özgökmen, T.M., Poulain, P.-M., 2001. Prediction of particle trajectories in the Adriatic Sea using Lagrangian data assimilation. *J. Mar. Sys.* 29 (1–4), 33–50.
- Coulliette, C., Wiggins, S., 2000. Intergyre transport in a wind-driven, quasigeostrophic double gyre: an application of lobe dynamics. *Nonlinear Proc. Geophys.* 7, 59–85.
- Cushman-Roisin, B., Gacic, M., Poulain, P.-M., Artegiani, A., 2001. *Physical oceanography of the Adriatic Sea: past, present and future.* Kluwer Academic Publishers.
- Davis, R., 1991. Observing the general-circulation with floats. *Deep-Sea Res.* 38, 531–571.
- Egbert, G.D., Erofeeva, S.Y., 2003. Efficient inverse modeling of barotropic ocean tides. *J. Atmos. Ocean. Tech.* 19, 183–204.
- Falco, P., Griffa, A., Poulain, P.M., Zambianchi, E., 2000. Transport properties in the Adriatic Sea as deduced from drifter data. *J. Phys. Oceanogr.* 30, 2055–2071.
- Farmer, R., Pawlowicz, D., Jiang, R., 2002. Tilting separation flows: a mechanism for intense vertical mixing in the coastal ocean. *Dyn. Atmos. Ocean.* 36, 43–58.
- Flather, R.A., Proctor, R., 1983. Prediction of North Sea Storm Surges using Numerical Models: Recent Developments in the UK. In: Sundermann, J., Lenz, W. (Eds.), *North Sea Dynamics.* Springer, New York.
- Fratantoni, D., 2001. North Atlantic surface circulation during the 1990's observed with satellite-tracked drifters. *J. Geophys. Res.* 106, 22067–22093.
- Garraffo, Z.D., Mariano, A.J., Griffa, A., Veneziani, C., Chassignet, E.P., 2001. Lagrangian data in a high-resolution numerical simulation of the North Atlantic. 1. Comparison with in situ drifter data. *J. Mar. Sys.* 29, 157–176.
- Griffa, A., 1996. Applications of stochastic particle models to oceanographic problems. In: Adler, R., Müller, P., Rozovskii, B. (Eds.), In: *Stochastic modelling in Physical Oceanography*, 467. Birkhauser, Boston, pp. 113–128.
- Griffa, A., Piterbarg, L.I., Özgökmen, T.M., 2004. Predictability of Lagrangian trajectories: effects of uncertainty in the underlying Eulerian flow. *J. Mar. Res.* 62 (1), 1–35.
- Haller, G., Poje, A., 1998. Finite time transport in aperiodic flows. *Physica D* 119, 352–380.
- Hodur, R.M., 1997. The naval research laboratory's coupled ocean/atmosphere mesoscale prediction system (COAMPS). *Mon. Wea. Rev.* 125, 1414–1430.
- Holland, W.R., Chow, J.C., Bryan, F.O., 1998. Application of a third-order upwind scheme in the NCAR ocean model. *J. Clim.* 11, 1487–1493.
- Kantha, L.H., Clayson, C.A., 2000. *Numerical Models of Oceans and Oceanic Processes.* Academic Press, California, p. 883.
- Kolmogoroff, A.N., 1941. The local structure of turbulence in an incompressible viscous fluid for very large Reynolds number. *C. R. Acad. Sci. USSR* 30, 301–305.
- LaCasce, J.H., Bower, A., 2000. Relative dispersion in the subsurface North Atlantic. *J. Mar. Res.* 58, 863–894.
- LaCasce, J.H., Ohlmann, C., 2003. Relative dispersion at the surface of the Gulf of Mexico. *J. Mar. Res.* 61, 285–312.
- Lavender, K., Davis, R., Owens, W., 2002. Observations of deep convection in the Labrador Sea from subsurface floats. *J. Phys. Oceanogr.* 32, 511–526.
- Martin, P.J., 2000. A Description of the Navy Coastal Ocean Model Version 1.0. NRL Report NRL/FR/7322-00-9962, Naval Research Laboratory, SSC, MS 39529, p. 42.
- Maurizi, A., Griffa, A., Poulain, P.M., Tampieri, F., 2004. Lagrangian turbulence in the Adriatic Sea as computed from drifter data: effects of inhomogeneity and nonstationarity. *J. Geophys. Res. Oceans*, 109, Art. No. C04010.
- McClellan, J.L., Poulain, P.-M., Pelton, J.W., 2002. Eulerian and Lagrangian statistics from surface drifters and a high-resolution POP simulation in the North Atlantic. *J. Phys. Oceanogr.* 32, 2472–2491.
- Mellor, G.L., 1991. An equation of state for numerical models of oceans and estuaries. *J. Atmos. Ocean. Tech.* 8, 609–611.
- Mellor, G.L., Yamada, T., 1974. A hierarchy of turbulence closure models for planetary boundary layers. *J. Atmos. Sci.* 31, 1791–1806.
- Miller, P., Pratt, L., Helfrich, K., Jones, C., 2002. Chaotic transport of mass and potential vorticity for an island recirculation. *J. Phys. Oceanogr.* 32, 80–102.
- Molcard, A., Piterbarg, L., Griffa, A., Özgökmen, T.M., Mariano, A.J., 2003. Assimilation of drifter positions for the reconstruction of the Eulerian circulation field. *J. Geophys. Res. Ocean.* 108 (3), 3056. doi:10.1029/2001JC00124.
- Molcard, A., Poje, A.C., Özgökmen, T.M., 2006. Directed drifter launch strategies for Lagrangian data assimilation using hyperbolic trajectories. *Ocean Modell.* 12, 268–289.
- Morey, S.L., Martin, P.J., O'Brien, J.J., Wallcraft, A.A., Zavala-Hidalgo, J., 2003. Export pathways for river discharged fresh water in the Northern Gulf of Mexico. *J. Geophys. Res.* 108 (1), 1–15.
- Orlanski, I., 1976. A simple boundary condition for unbounded hyperbolic flows. *J. Comp. Phys.* 21, 251–269.
- Owens, W., 1991. A statistical description of the mean circulation and eddy variability in the northwestern Atlantic using SOFAR floats. *Prog. Oceanogr.* 28, 257–303.
- Özgökmen, T.M., Griffa, A., Piterbarg, L.I., Mariano, A.J., 2000. On the predictability of Lagrangian trajectories in the ocean. *J. Atmos. Ocean. Technol.* 17 (3), 366–383.
- Özgökmen, T.M., Piterbarg, L.I., Mariano, A.J., Ryan, E.H., 2001. Predictability of drifter trajectories in the tropical Pacific Ocean. *J. Phys. Oceanogr.* 31, 2691–2720.
- Pawlak, G., MacCreedy, P., Edwards, K.A., McCabe, R., 2003. Observations on the evolution of tidal vorticity at a stratified deep water headland. *Geophys. Res. Lett.* 30 (24), 2234. doi:10.1029/2001JC00123.

- Pinardi, N., Allen, I., Demirov, E., De Mey, P., Korres, G., Lascaratos, A., Le Traon, P.-Y., Maillard, C., Manzella, G., Tziavos, C., 2003. The Mediterranean ocean forecasting system: first phase of implementation (1998–2001). *Ann. Geophys.* 21, 3–20.
- Piterbarg, L.I., 2001a. The top Lyapunov exponent for a stochastic flow modeling the upper ocean turbulence. *SIAM J. Appl. Math.* 62 (3), 777–800.
- Piterbarg, L.I., 2001b. Short term prediction of Lagrangian trajectories. *J. Atmos. Ocean. Technol.* 18 (8), 1398–1410.
- Poje, A., Haller, G., 1999. Geometry of cross-stream mixing in a double-gyre ocean model. *J. Phys. Oceanogr.* 29, 1649–1665.
- Poje, A.C., Toner, M., Kirwan, A.D., Jones, C.K.R.T., 2002. Drifter launch strategies based on Lagrangian templates. *J. Phys. Oceanogr.* 32, 1855–1869.
- Poulain, P.-M., 1999. Drifter observations of surface circulation in the Adriatic Sea between December 1994 and March 1996. *J. Mar. Sys.* 20, 231–253.
- Poulain, P.-M., 2001. Adriatic Sea surface circulation as derived from drifter data between 1990 and 1999. *J. Mar. Sys.* 29, 3–32.
- Pullen, J., Doyle, J.D., Hodur, R., Ogston, A., Book, J.W., Perkins, H., Signell, R., 2003. Coupled ocean–atmosphere nested modeling of the Adriatic Sea during winter and spring 2001. *J. Geophys. Res.* 108 (C10), 3320. doi:10.1029/2003JC00178.
- Raicich, R., 1994. Note on the flow rates of the Adriatic rivers, Technical Report RF 02/94, Consiglio Nazionale delle Ricerche Istituto Sperimentale Talassografico, Trieste, Italy, p. 8.
- Reverdin, G., Niiler, P., Valdiimasson, H., 2003. North Atlantic Ocean surface currents. *J. Geophys. Res.* 108, 3002.
- Reynolds, A.M., 2002. Lagrangian stochastic modeling of anomalous diffusion in two-dimensional turbulence. *Phys. Fluids* 14, 1442–1449.
- Reynolds, A.M., 2003. Third-order Lagrangian stochastic modeling. *Phys. Fluids* 15, 2773–2777.
- Richardson, P., 2001. Drifters and floats. *Encyclopedia Ocean Studies* 2, 767–774.
- Rosmond, T.E., Teixeira, J., Peng, M., Hogan, T.F., Pauley, R., 2002. Navy operational global atmospheric prediction system (NOGAPS) forcing for ocean models. *Oceanography* 15, 99–108.
- Sagaut, P., 2005. Large eddy simulation for incompressible flows. Springer, p. 319.
- Shay, L., Cook, T., Haus, B., Martinez, J., Peters, H., Mariano, A., VanLeer, J., An, P., Smith, S., Soloviev, A., Weisberg, R., Luther, M., 2000. VHF radar detects oceanic submesoscale vortex along Florida coast. *Eos Trans.* 81, 209–213.
- Smith, R.D., Maltrud, M.E., Bryan, F.O., Hecht, M.W., 2000. Numerical simulation of the North Atlantic ocean at 1/10 °. *J. Phys. Oceanogr.* 30, 1532–1561.
- Taylor, G.I., 1921. Diffusion by continuous movements. *Proc. London Math. Soc.* 20, 196–212.
- Taillandier, V., Griffa, A., Paoulain, P.M., Beranger, K., 2006. Assimilation of Argo float positions in the north western Mediterranean Sea and impact on ocean circulation simulations. *Geophys. Res. Lett.*, 33/11, Art. No. L11604.
- Thomson, D.J., 1986. A random walk model of dispersion in turbulent flows and its application to dispersion in a valley. *Quat. J. R. Met. Soc.* 112, 511–529.
- Toner, M., Poje, A.C., 2004. Lagrangian velocity statistics of directed launch strategies in a Gulf of Mexico model. *Nonlin. Proc. Geophys.* 11, 35–46.
- Veneziani, M., Griffa, A., Reynolds, A.M., Mariano, A.J., 2004. Oceanic turbulence and stochastic models from subsurface Lagrangian data for the North-West Atlantic Ocean. *J. Phys. Oceanogr.* 14, 1884–1906.
- Veneziani, M., Griffa, A., Garraffo, Z.D., Chassignet, E.P., 2005a. Lagrangian spin parameter and coherent structures from trajectories released in a high-resolution ocean model. *J. Mar. Res.* 63 (4), 753–788.
- Veneziani, M., Griffa, A., Reynolds, A.M., Garraffo, Z.D., Chassignet, E.P., 2005b. Parameterizations of Lagrangian spin statistics and particle dispersion in the presence of coherent vortices. *J. Mar. Res.* 63 (6), 1057–1083.
- Weissel, J.K., Pratson, L.F., Malinverno, A., 1994. The length-scaling properties of topography. *J. Geophys. Res.* 99 (B7), 13997–14012.
- Wiggins, S., 2005. The dynamical systems approach to Lagrangian transport in oceanic flows. *Ann. Rev. Fluid. Mech.* 37, 295–328.
- Zhang, H., Prater, M., Rossby, T., 2001. Isopycnal Lagrangian statistics from the North Atlantic Current RAFOS float observations. *J. Geophys. Res.* 106, 13817–13836.
- Zhou, M., Niiler, P., Hu, J., 2002. Surface currents in the Bransfield and Gerlache straits. *Atlantica Deep Sea Res.* 49, 267–280.